Reconstructing the Fluvial History of the Lilas River (Euboea Island, Central West Aegean Sea) from the Mycenaean Times to the Ottoman Period

Matthieu Ghilardi, Tim Kinnaird, Katerina Kouli, Andrew Bicket, Yannick Crest, François Demory, Doriane Delanghe, Sylvian Fachard, David Sanderson

geosciences

MDPI

Article

Reconstructing the Fluvial History of the Lilas River (Euboea Island, Central West Aegean Sea) from the Mycenaean Times to the Ottoman Period

Matthieu Ghilardi [1,*], Tim Kinnaird [2], Katerina Kouli [3], Andrew Bicket [4], Yannick Crest [1], François Demory [1], Doriane Delanghe [1], Sylvian Fachard [5] and David Sanderson [6]

1 Centre Européen de Recherches et D'enseignement des Géosciences de l'Environnement (CEREGE), Aix-Marseille University—UMR 7330 CNRS—IRD—Collège de France—INRAE, Europôle Méditerranéen de l'Arbois BP 80, CEDEX 04, 13545 Aix-en-Provence, France; yannickcrest@laposte.net (Y.C.); demory@cerege.fr (F.D.); delanghe@cerege.fr (D.D.)
2 School of Earth and Environmental Sciences, University of St Andrews, St Andrews KY16 9TS, UK; tk17@st-andrews.ac.uk
3 Department of Geology and Geoenvironment, National and Kapodistrian University of Athens, Panepistimiopolis, 15784 Zographou, Greece; akouli@geol.uoa.gr
4 Wessex Archaeology, 21-23 Slater's Steps, Edinburgh EH8 8PB, UK; a.bicket@wessexarch.co.uk
5 Swiss School of Archaeology in Greece, University of Lausanne, ASA—Bâtiment Anthropole, CH-1015 Lausanne, Switzerland; sylvian.fachard@unil.ch
6 Scottish Universities Environmental Research Centre (SUERC), University of Glasgow, Glasgow G75 OQF, UK; David.Sanderson@glasgow.ac.uk
* Correspondence: ghilardi@cerege.fr; Tel.: +33-4-13-94-92-09

Abstract: This paper aims to reconstruct the alluvial activity for the Lilas river, the second-largest catchment of Euboea Island (Central Western Aegean Sea), for approximately the last three and a half millennia. The middle reaches (Gides basin) exhibit several historical alluvial terraces that were first recognised in the 1980s but have remained poorly studied, resulting in uncertain chronological control of palaeofluvial activity. In order to reconstruct the past fluvial dynamics of the Lilas river, a ca. 2.5 m thick stratigraphic profile has been investigated for granulometry and magnetic parameters. Absolute dating of the sediments was possible by applying Optically Stimulated Luminescence (OSL). The results reveal: (i) two coarse-grained aggradational episodes dated from the Mycenaean/Early Iron Age and the Roman periods, respectively, (ii) a phase of rapid fine-grained vertical accretion corresponding to the Late Byzantine to early Venetian periods, (iii) potential evidence for final alluvial deposition from the Little Ice Age/Ottoman period, and (iv) two major incision episodes inferred from Ancient Greek times and most of the Byzantine period. Based on the published core material, the paper also evaluates the direct impacts of the Late Holocene alluviation recorded mid-stream on the fluvial system situated downstream in the deltaic area. Sediment sourcing is attempted based on the magnetic properties of the catchment lithology and of alluvium collected upstream along the main stream bed. Finally, the present paper discusses the possible links between Late Holocene hydroclimatic oscillations and the aggradational/incision phases revealed in the Gides basin. Correlations are attempted with regional palaeoclimate records obtained for the Aegean. In addition to climatic variability, anthropogenic factors are considered: specific land use for agricultural purposes, in particular during the Mycenaean period, the Roman and the Late Byzantine/Early Venetian periods, might have enhanced sediment deposition. Archaeological information and pollen records were also evaluated to reconstruct regional land-use patterns and possible impacts on soil accumulation over the last 3.5 millennia.

Keywords: Euboea Island; Greece; Lilas river; OSL dating; stratigraphic profile; granulometry; magnetic parameters; Late Holocene

Citation: Ghilardi, M.; Kinnaird, T.; Kouli, K.; Bicket, A.; Crest, Y.; Demory, F.; Delanghe, D.; Fachard, S.; Sanderson, D. Reconstructing the Fluvial History of the Lilas River (Euboea Island, Central West Aegean Sea) from the Mycenaean Times to the Ottoman Period. *Geosciences* **2022**, *12*, 204. https://doi.org/10.3390/geosciences12050204

Academic Editors: Tina Wunderlich, Peter Fischer and Jesus Martinez-Frias

Received: 21 March 2022
Accepted: 5 May 2022
Published: 11 May 2022

1. Introduction

Alluvial geoarchaeology in the Mediterranean has, for the last 50 years, emphasised both natural and anthropogenic factors as the main drivers to phases of vertical sediment accretion and incision during the Holocene [1]. Following the major work published by C. Vinta-Finzi [2] with the identification of the so-called "younger fill" (5000–400 BP) [3], associated with climate control on the sedimentation during the Roman period, the role played by human societies in terms of sediment accumulation/erosion has subsequently been demonstrated [4–9]. Over the last decades, significant advances have been made in identifying and timing different phases of alluviation during the Late Holocene, using different techniques for absolute dating of stratigraphic sections or core sequences that contained detrital material (archaeological markers and OSL/^{14}C dating techniques).

Mainland Greece has been extensively studied for reconstructing Mid- to Late Holocene fluvial environments using cross-disciplinary archaeological evidence and paleoenvironmental data, e.g., in the Peloponnese (south Greece [10–13], in Epirus [14], in central and eastern Macedonia (north central-west Greece) [8,9,15–17]). In most palaeofluvial studies, OSL dating is rarely used, except in the Peloponnese to date flooding activity over the last millennium [18]. Little alluvial geoarchaeology research has been undertaken on the Aegean islands, except in Euboea and Crete. Of the work that has been conducted, OSL was used to date phases of sediment accretion in Crete [19–21]. In particular, Macklin et al. (2010) defined a robust geochronology for the Anapodaris (south-central Crete) fluvial environments for the Late Holocene [19]: first, an aggradational episode of coarse material from c. 3400 to 3000 BP; then, finer-grained alluvial sedimentation during the Roman period (c. 2000 BP) and at different dates around the onset of the 2nd millennium CE.

Results from the Istron area, east-central Crete (Figure 1) [20], highlighted a massive vertical sedimentary accretion related to the Wet and Warm Roman Climatic Optimum (40 to 60 cm/century; [20]). Theodorakopoulou et al. [21] defined this further, revealing a new phase of vertical accretion in eastern Crete in the Late Byzantine period (Figure 1 [21]).

Apart from these valuable works conducted in Crete, alluvial geoarchaeological studies remain scarce in the Aegean islands and only concern the small catchments (<40 km^2) from Thasos Island (North-Central Aegean), where strong alluviation has been notably evidenced for Roman times and the Byzantine period [9]. For Euboea, palaeofluvial research is also scarce and general, focusing on the relationships between active neotectonics and the formation of alluvial terraces [22,23]. Only one study in south Euboea [24] documents alluviation (mostly during Roman and Late Byzantine times), but the paucity of the radiocarbon dating does not allow a full environmental reconstruction. In addition, dating the fluvial input using radiocarbon dating of organic matter embedded within sediments remains uncertain due to contamination or reworked organic material during sedimentation processes [25–29]. For the central part of the island, through which the Lilas river runs, Genre [23,30] documented a series of fluvial aggradation/incision episodes during the historical period, based primarily on the identification of archaeological material embedded within the sediments. However, because the latter study lacked robust chronology, the correlations between climate, sediment dynamics and human occupation were only inferred.

The present study deals with the Mycenaean (Late Bronze Age), Roman, Venetian, and Ottoman periods, for which we relate phases of sediment accretion to human activity on the island by linking landscape dynamics, palaeoenvironmnetal investigations, and archaeology. It aims to address the dynamic interchanges between climate and human activity on the formation and erosion of alluvial terraces of the Lilas catchment; then, through extrapolation, comment on the reconstruction of Holocene alluvial dynamics across the Aegean basin at the catchment scale.

Figure 1. Geological map of the Lilas drainage basin. Geological data derived from 1/50,000 scale IGME geological maps. Black squares: archaeological sites mentioned in the text; grey squares: modern towns in the Lilas drainage basin; red circles: sedimentological cores obtained along the South Evoikos Gulf: A, B, C and D [31]; E and F [32]. Digital Elevation model derived from SRTM data (WGS 84 projection datum). In the inset map: stars indicate the location of palaeoclimate archives (in blue, marine core and light purple, speleothems); yellow squares indicate the location of palaeofluvial studies and orange polygons, the position of full pollen sequence. 1: M2 core [33,34]; 2: LC21 core [35]; 3: Skala Marion Cave (Thasos island [36]); 4: Kapsia cave (Peloponesus [37]); 5: Alepotrypa cave (Peloponnese [38]); 6: Paximadhi peninsula [24]; 7: Istron Bay [20] and Xeropotamos River [21]; 8: Anapodaris river [19]; 9: Vravron coastal swamps.

2. Site Setting

2.1. Topography, Geology and Tectonics

Euboea is the second largest island in Greece (after Crete). It is located northeast of Athens (Figure 1). The island has an area of 3684 km^2 and is c. 180 km in length. The highest summit, Mount Dirfys, reaches an elevation of 1743 m above sea level (Figures 1 and 2). The island broadly follows a northwest-southeast orientation and is separated from the Greek mainland by the narrow strait of "Euripos". Its relief is characterised by a series of mountainous ranges, which follow the NW–SE trend, separated by wide plateaus.

The island is divided into a series of small catchments: The largest is the Kirefs-Nirefs basin (c. 450 km^2); the second is the Lilas basin at c. 275 km^2. The latter has intermittent streamflow and is totally dry during summer. Despite this seasonal flow, the Lilas has been creating a prograding delta in the South Evoïkos Gulf since the Mid-Holocene [22,30–32].

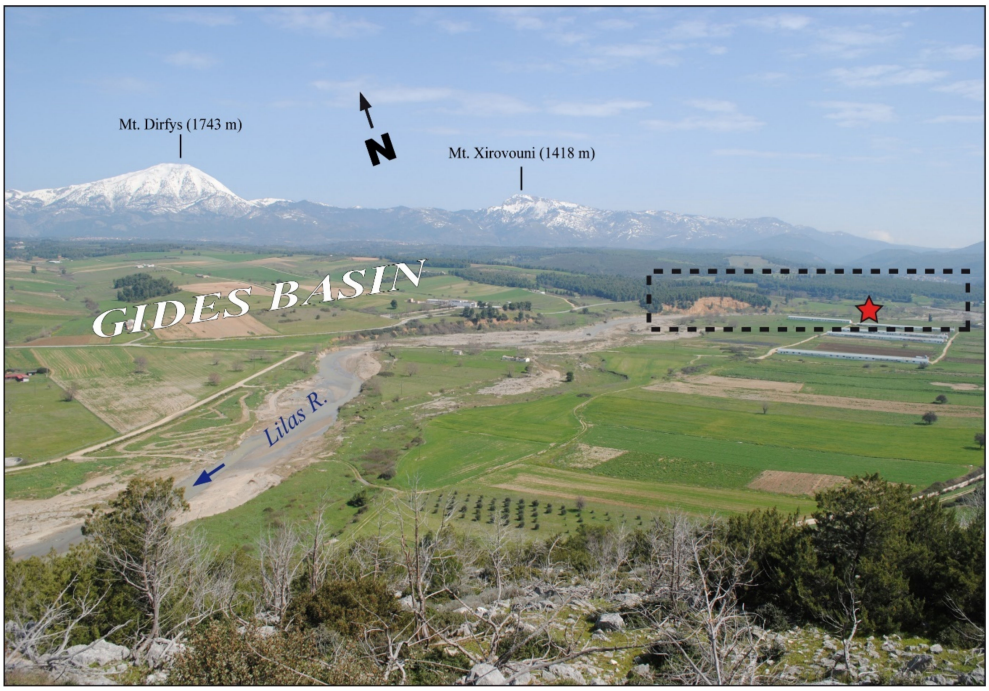

Figure 2. View to the north of the Lilas river in the area of Pissonas, Gides basin (March 2010). The rectangular area limited by a dashed line corresponds to the investigated area; terrace geometry is reported in Figure 3. The red star indicates the location of the studied profile.

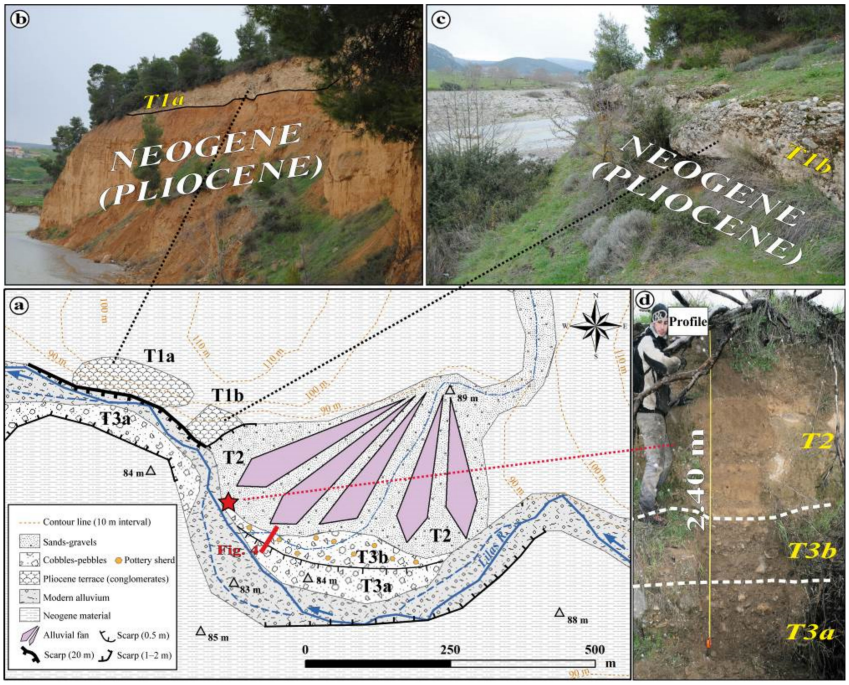

Figure 3. (**a**) Morphostructural mapping and terraces geometry. Topographic information is derived from 1:5000 scale maps. The red line indicates the position of the cross section revealing the terraces T3a, T3b and T2 (Figure 4); the red star indicates the position of the studied profile (**d**); Pliocene terraces are reported on (**b**,**c**).

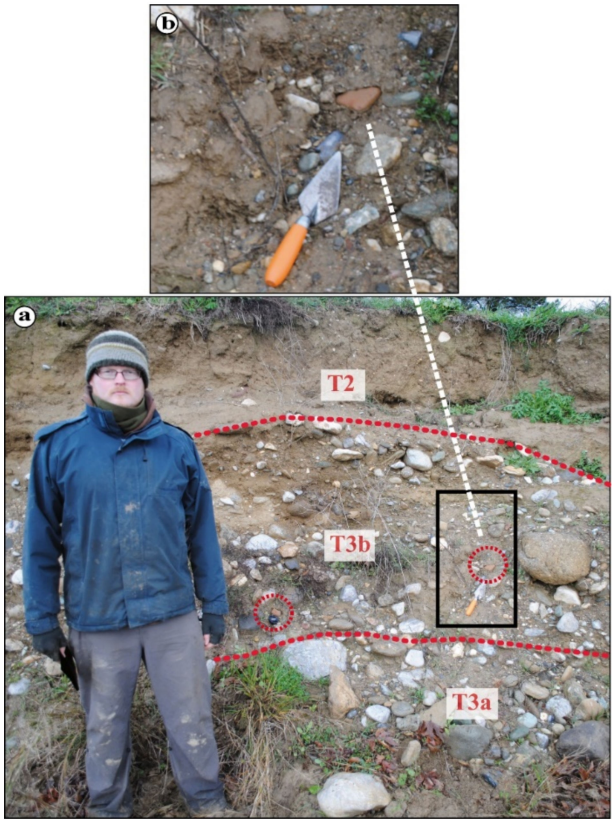

Figure 4. Cross section within the alluvial terraces deposits situated on the right bank of the Lilas river; refer to Figure 3a for exact location; (**a**) view of the different levels of alluvial terraces; (**b**) presence of rounded archaeological material (approx. 5 cm in length and of orange colour) embedded within alluvial terrace T3b sediments (in the picture: A. Bicket).

It is noteworthy that the only rivers associated with active deltas on the island are the Kallas (North Euboea) and Lilas rivers, both of which are associated with fan deltas [32]. There are several explanations for this, including Holocene active tectonism [22,23,39] and climate and anthropogenic impacts on the environment. With regard to the first, northern Euboea has been affected by constant tectonic uplift throughout the Holocene [40,41]. However, the south Euboean Gulf (South Evoikos Gulf; Figure 1) is an area of mild tectonic activity and moderate seismicity [42]. In addition, there are no large tectonic structures in the vicinity of the central Euboean Gulf, and earthquakes are usually of low magnitude. Historical earthquakes notably affected Chalkis and its immediate surroundings, but most of them had a little wider impact [43–45].

The geology of the catchment (Figure 1) can be divided into four zones [32]: The Dirfys/Xirovouni mountain range is formed from metamorphic (black schists, phyllites, marbles, and flysches) and carbonate rocks (pre-Neogene); the Gides basin (study area; Figure 2) is composed of Pliocene lacustrine to fluvio-lacustrine deposits, and characterised by deep gullies cut into this poorly consolidated substrate; further west and southwest, the Lilas dissects a hilly range comprised of Mesozoic ophiolites and limestones (Figure 1); and by the coast, Late Quaternary fan deltas formed directly in response to sea-level oscillations during the Pleistocene and Holocene.

Previous research on the Lilas river fan delta has revealed, since the Mid-Holocene, a progradation of the delta [31,32], with distinct phases of progradation (and lateral migration of the river mouth in an E/W direction) during the Roman-Byzantine, Venetian, and Ottoman periods [31]. Erosion of the unconsolidated lithology of the Gides basin, composing approximately a third of the sediments of the catchment [32], may explain this alluviation. Reconstructing the fluvial activity at the scale of the drainage basin is

challenging. To overcome this, we have combined studies of the alluvial terraces in the mid-catchment with studies of the deltaic sediments at the coast.

2.2. Alluvial Terraces Geometry

In the Gides basin, 2 km SE of Pissonas (situated at the midpoint of the Lilas river course; Figures 1 and 2), three main topographic levels of alluvial terraces were observed (Figure 3):

The highest topographic alluvial terrace is situated ca. 25 m above the present-day river course (T1a): it is composed of cemented (white to light grey colour) rounded pebbles, gravels and sands, and overlays Neogene deposits. This terrace is likely to be (earlier) Pliocene in age since it is bracketed by oxidised limnic silts, relevant to the late Neogene formation of the Gides basin (Figure 1).

A sub-terrace of T1, T1b is situated 5 to 7 m above the present-day river course and is mainly composed of cemented (carbonate matrix) angular and rounded pebbles and sands. It shows the same features as T1a and therefore is associated with a phase of alluviation during the Pliocene.

The second level of terrace T2 (Figures 3 and 4) is situated below Unit T1b, between 1.5 and 2.5 m above the present-day river bed and is associated with a small fan created by a local stream located on the right embankment of the river (Figure 3). The sediment is generally fine-grained, with occasional intercalations of gravels and dark organic bands (more so towards the top of the unit). There are no archaeological artefacts in Unit 2.

The third level of alluvial terrace T3 (Figures 3 and 4) is situated above the actual main river course channel, no more than 1.5 m from the modern course of the river. It is divided into two sub-units: T3a is formed from pebbles and large cobbles (ca. 10 to 20 cm in length) within a sandy matrix. No archaeological material was found. T3a might have been deposited within the context of high river transport capacity associated with a fluvial braided river system. Directly overlying T3a is a second unit, T3b, with a similar granulometry to T3a (Figure 4a), large rounded pebbles bound in a sandy matrix but with a low representation of the larger cobbles. Moreover, artefacts, mostly fragmentary and rounded pottery, are present (orange colour; Figure 4b). Due to low preservation, precise dating of these artefacts is problematic; but they likely date to Antiquity rather than Pre- or Proto-history. The transition between T3a and T3b is marked by thin layers of sands in some areas, as in the studied sedimentary profile (Figure 3d).

Terrace deposits T2, T3a and T3b are dated to the Holocene; samples for OSL dating were collected throughout these deposits (Figure 3d) to provide the temporal framework to reconstruct the Mid- to Late Holocene fluvial dynamics of the Lilas river and determine whether alluviation coincided with periods of intense land use in specific cultural periods.

2.3. Archaeological and Historical Background

During the Bronze Age (3000–1000 BCE), the region of Chalkis was occupied by several significant sites [46], attracted by the strategic position of the Euripos strait and the extraordinary agricultural potential of the Lilas basin, in particular the Lelantine Plain. In the first millennium BCE, the Early Iron Age saw the emergence of the city-states of Chalkis and Eretria [47–49]. Unfortunately, no systematic archaeological research has been conducted in the Lilas basin since the British survey of the 1960s [50]. Therefore, despite its great significance in terms of agriculture and settlement, the Lilas catchment remains poorly known from an archaeological point of view. Several Middle to Late Bronze Age sites are located in the Voudochi mountain range which forms the southernmost part of the Lilas catchment (Figure 5). Occupation during the Mycenaean period (1600–1200 BCE) is also evidenced in the Gides basin at Mistros (Figure 5). Human occupation progressively increased in central Euboea in the Early Iron Age and reached a peak in the Classical and Early Hellenistic periods, when the Lilas river was controlled by the polis of Chalkis [51]. Sites are known at Pissonas and Aghioi, but many more settlements must have existed in this fertile area. Chalkis was the most significant town in Euboea in the 1st–2nd centuries CE when the city enjoyed a relative period of prosperity. In the Early Byzantine period, the

town of Chalkis moved to the west to control the Euripos, after which the new city was named [52]. The city belonged to the Theme of Hellas and became one of Greece's most important fortified towns [46]. From the 10th–12th centuries CE, Byzantine Emperors granted several privileges to the Venetians, while a Jewish community is known from 1160 CE.

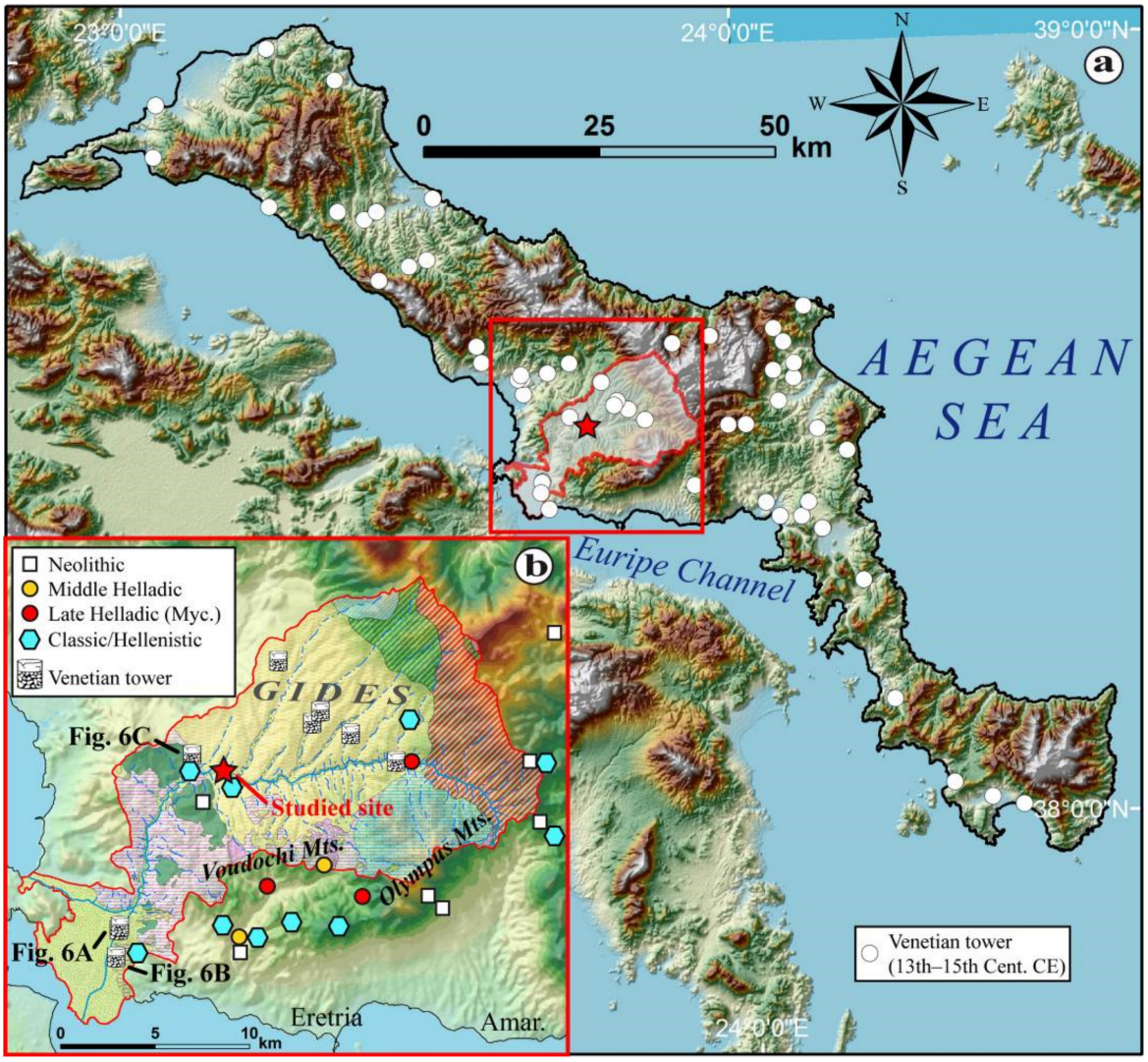

Figure 5. Archaeological map of the study area; (**a**) Location map of the Venetian towers (13th–15th Cent. CE) identified for Euboea Island [53]; (**b**) location map of the archaeological sites situated in the Lilas catchment and around it.

The conquest of Constantinople by the Latins of the Fourth Crusade (1204 CE), and the subsequent distribution of the Byzantine territories among the victors, meant that the island remained under Latin domination for a long period of time [54]. The city of Euripos was renamed Negroponte. During the following Venetian period, Euboea experienced a period of demographic prosperity. Its strategic location in the middle of trade routes in the Aegean rendered the island one of the principal trading ports for Venetian ships. Until the 14th cent. CE, Venice had been able to extend its direct domination over a large part of the island through purchases and conquests of fortresses. The Latin rulers also imported a fundamental part of the Western feudal system: the idea of the feudal tower. This is demonstrated by the remains of 55 single isolated towers in the countryside of Euboea, dated to the period of Latin rule (1205–1470 CE [55]). Most of the towers were built in areas with extensive fertile agricultural land and were free-standing constructions (Figure 6a–c). They were not associated with other buildings of any kind, such as defensive

walls or other structures. They were tall and massive rectangular buildings with an average height of between 15 and 18 m (Figure 6a) and were constructed between the 13th and 15th cent. CE. These striking landmarks, stemming from the Western feudal system, served as residences for the local feudal lord and functioned as administrative and agricultural centres of the fief. In 1470, Negroponte was besieged and then conquered by the Ottomans, who ruled until 1830 CE. The Ottoman census of the end of the 15th century showed a dense occupation in the Lilas catchment, in particular, around the Gides basin, which belonged to the *Nahiye* of Agalyos [56]: Yidez (Amphithea, 27 houses), Vunuz (Vounoi, 93 houses), Kanbiya (Kambia, 14 houses), and Istin (Steni, 34 houses). In the 17th century, the Ottomans built a long aqueduct traversing the Gides basin, exploiting a spring at Ano Kambia, on the slopes of Mt. Dirfys [57].

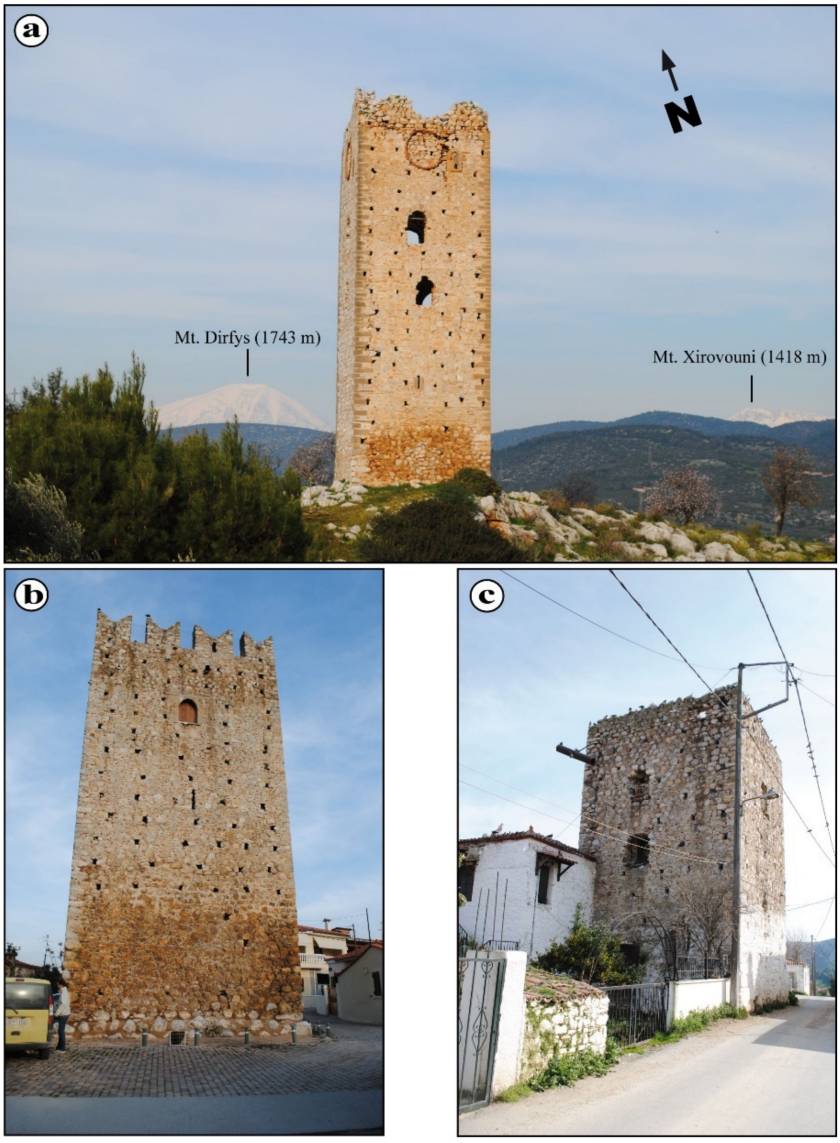

Figure 6. Venetian towers exist at (**a**) Phylla; (**b**) Vassiliko (lower reaches of the Lilas river) sand; and (**c**) at Pissonas.

2.4. A Review of the Palaeoclimate and Fluvial Reconstructions Obtained for the Central Aegean Sea Covering the Last Three Millennia

Over the last decade, palaeoclimate reconstructions for the Holocene have been established for the whole Mediterranean [58–60], based on the compilation of regional studies mainly derived from speleothem or sedimentary archives studies.

No palaeoclimatic studies have been undertaken on Euboea, and it is, therefore, necessary to refer to proxy data from the surrounding areas. Fortunately, a rich literature exists for the North Aegean basin based on speleothems (Thasos Island [36]), marine cores [33,61], terrestrial archives [62], and combinations of the latter [63]. From the south, palaeoclimate reconstructions exist for the Peloponnese based on speleothems [37,38,64] and lake sediments [65,66]. In addition, a study of a marine core covering part of the last three millennia is available in eastern Crete [35]. Here, the main palaeoclimate trends are summarised, although some contradictory evidence exists, as noted by Finné et al. [59].

From 3400 to 2700 cal. BP, wet conditions are reported in the North Aegean, with a humid peak recorded around 3200 cal. BP [36]. In contrast, Central and South Aegean, as well as Peloponnese, experienced dry conditions for the same period [59], with a cold period at around 3000–2900 BP [35]. However, palaeoenvironmental studies derived from boreholes studies for the central Peloponnese revealed a period of more humid and cooler conditions at the same time [67]. Further south, on Crete, Macklin et al. [19] document aggradational episode(s) between 3400–3000 cal. BP, reflecting wet conditions.

From 2600 to 2000 cal. BP, dry conditions prevailed both in the North Aegean [36] and in the South Aegean Sea [37,67], with maximum aridity at c. 2300 cal. BP [36]. This dry period was first reported on a regional scale in the Levant [68,69]. As a direct consequence, local vegetation cover was reduced, as reported in Attica [70] and southern Crete [71]. However, the sharp decrease of Arboreal Pollen (AP) percentages that affected the North Aegean, culminating at ~2200 cal. BP, was not attributed to climate control. Instead, it appears to have resulted from anthropogenic influence on vegetation [63].

From 1900 to 1500 cal. BP, humid conditions are reported in the North Aegean Sea [36] and South Greece [20,72], corresponding to the Wet and Warm Roman Optimum (WRO). As a direct consequence, enhanced fluvial activity is reported for the Aegean islands, including south Euboea [24] and Crete [19,20]. Palaeofluvial studies conducted on the Greek mainland [73] also report fluvial activity around the WRO.

The second half of the first millennium CE, starting from ca. 1700 cal. BP [61,74], is characterised in the North Aegean Sea by more arid conditions, with the peak reached at c. 1400 cal. BP (CE 550 [36]). Such arid conditions lasted until 1250 cal. BP both in the Aegean and Eastern Mediterranean, in general (CE 750 [75]). This dry and cold event is known as the Dark Ages Cold or Bond 1 event [20]. The Late Byzantine period is recognised in Greece as a major phase of detrital activity, especially in the Peloponnese (southern Greece [10,12,76]), eastern Macedonia (north-eastern Greece [8]), Crete (South Aegean [19,21]), and southern Euboea (central Greece [24,73]).

For the last 1000 years, very accurate paleoclimate reconstructions with a centennial resolution have been generated for the North Aegean Sea and the broader NE Mediterranean [58,77]. In the North Aegean, humid and warm conditions prevailed from ca. 950 to 650 cal. BP [34,62] with important alluvial activity [33]. Such particularly wet conditions have also been reported for the South Aegean ca. 1050–850 cal. BP [34] and in Crete in particular [19–21]. In general, the entire Eastern Mediterranean (Greece, Anatolia, and the Middle East) experienced a peak in wet conditions at around 750 cal. BP [58]. This wet and warm period corresponds to the Medieval Climate Anomaly [33,34]. Following this, drier conditions prevailed from ca. 700–550 cal. BP, with a return to wet conditions after 500 cal. BP (peak at 350 cal. BP) in the Northern Aegean during the Little Ice Age [33]. Intense runoff associated with major fluvial flood events is reported in the North Aegean and in the whole NE Mediterranean, at 1000, 800, 500, and 350 cal. BP [33].

3. Field and Laboratory Methods

3.1. Field Sampling

On a right embankment of the Lilas river, the terraces of Holocene age, T3a, T3b and T2 were investigated. A profile measuring 2.40 m long was selected (Figure 3a,d) and cleaned for sampling; this permitted access to the full sequence of terrace deposits (Figure 3d). Within the different terrace levels, sedimentary units were recognised (Table 1) based first on visual observation of the lithology and general texture, then the subsequent laboratory analyses. All laboratory analyses performed on the sediments are reported in Table 1.

Table 1. Summary of the laboratory works conducted on the different sedimentary units from the studied profile.

Terrace Level	Sedimentary Unit	Granulometry	Magnetic Susceptibility	OSL Dating	Archaeological Material
T2	Unit IV	Manual sieving + LASER	Yes	No	No
	Unit III	Manual sieving + LASER	Yes	Yes	No
T3b	Unit II	Manual sieving	Yes	Yes	Yes
T3a	Unit I	Manual sieving + LASER	Yes	Yes	No

3.2. Magnetic Susceptibility Measurements

Magnetic susceptibility measurements were performed using the MFK1 magnetic susceptibility meter (Agico) at CEREGE (Aix-en-Provence, France). The sand fractions (matrix containing particles of <2 mm in size) were sampled along the profile at ~5 cm resolution, as shown in Figure 4, yielding 48 samples in total. These samples were placed in 8 cm^3 plastic boxes, dried, and weighed. In addition to the low-field magnetic susceptibility, typically measured at 976 Hz frequency, measurements were also taken at 15,616 Hz frequency. Magnetic susceptibility can be used as an indicator of the concentration of magnetic particles. This measurement includes the contribution from diamagnetic, paramagnetic and ferromagnetic particles, with high values mostly a reflection of ferromagnetic particle concentration (the size of the ferromagnetic particles can also influence magnetic susceptibility values). The magnetic susceptibility measurements performed at two frequencies are used to detect the ultrafine (<0.03 μm) superparamagnetic particles, which are produced by bacteria or chemical processes during soil formation [78,79].

Magnetic susceptibility of unconsolidated material is also applied to determine sediment sources within catchments presenting contrasting lithologies in terms of magnetic particles content [80], as has been demonstrated in small (<1000 km^2) Mediterranean drainage basins [81,82]. In the case of the Lilas river, the upper reaches cut metamorphic rocks to the north (Mt. Dirfys) and the northeast (Mt. Xirovouni range) (schists, flysches, and marbles; Figure 1), characterised by low magnetic particle content; whereas the southern catchment cuts both carbonate rocks (with low magnetic particles content) and eruptive rocks (with high magnetic signal, i.e., as in the Voudochi Mountain range (Figure 1)). The Gides basin, which incorporates the studied stratigraphic profile, has local tributaries of the Lilas river in its watershed that drain unconsolidated Neogene fluvio-limnic materials. Here, the presence of oxidised layers suggests high contents of magnetic particles. Situated downstream, ophiolites (Figure 1) and associated oxidised material (*Terra Rossa* deposits) exhibit a generally high concentration of magnetic particles. Sampling to characterise the magnetic susceptibility signal was also undertaken upstream of the sampled profile to encompass all of the different lithologies in the catchment.

3.3. Grain Size Analyses: Laser Granulometry and Manual Sieving Methods

Grain size determinations were conducted at CEREGE on the same samples analysed for the study of the magnetic parameters.

First, all sediment samples were wet-sieved in order to estimate the proportion of fine (<2 mm) and coarse (>2 mm) particle fractions. The percentage distribution by weight of fine-grained material (<2 mm) and gravels-pebbles (>2 mm) was estimated for each sample.

The fraction below 2 mm was subsequently studied for LASER granulometry. Some samples displayed significant organic matter content. The latter, when present in significant amounts, aggregates on clays changing the size distribution. Organic matter was removed using an H_2O_2 solution prior to the laser-diffraction particle size study [83,84]. The grain-size distribution was then measured using a Beckman Coulter LS 13,320 laser granulometer with a range of 0.04 to 2000 microns in 132 fractions. The calculation model (Beckman Coulter software version 5.01) uses Fraunhöfer and Mie theory. For the calculation model, we used water as the medium (RI = 1.33 at 20 °C), a refractive index in the range of kaolinite for the solid phase (RI = 1.56), and absorption coefficients of 0.15 for the 780-nm laser wavelength and 0.2 for the polarised wavelengths [83]. Samples containing fine particles were diluted with deionised water so that we measured between 8 and 12% of obscuration and between 45 and 70% Polarization Intensity Differential Scattering (PIDS) obscuration. Finally, statistical analyses were exported to GRADISTAT particle size analysis software [85].

3.4. OSL Profiling and Dating

All sample preparation and analysis were undertaken in the luminescence laboratories at SUERC following standard protocols [86,87]. Full details are provided in Kinnaird et al. [88]. A three-stage approach was utilised to appraise the sediment stratigraphy: first, the luminescence properties of bulk sediment were screened using portable OSL equipment; then, these samples (Table 2) were progressed to calibrated luminescence measurements in a Risø OSL-TL DA-15 reader to provide a first approximation of apparent doses; and finally, samples were progressed to quantitative quartz SAR OSL dating.

Table 2. Samples selected for OSL dating expressed according to the depth and indicative granulometry. Refer to Figure 7 for identification of the different levels of palaeosols.

SUERC Code	Field Number	Depth in Section (m)	Sedimentary Unit (Terrace Level)	Description
SUTL 2363	Lilas6	70	Unit III (Terrace T2)	Palaeosol P4
SUTL 2391	Lilas5	100	Unit III (Terrace T2)	Silty sands/palaeosol P3
SUTL 2362	Lilas4	130	Unit III (Terrace T2)	Palaeosol P2
SUTL 2361	Lilas2	155	Unit II (Terrace T3b)	Silts/fine-grained sands; brown to yellow/Palaeosol P1
SUTL 2390	Lilas 1	190	Unit I (Terrace T3a)	Silts to sands

Initial screening measurements were made using a Risø DA-15 luminescence reader on paired discs of quartz and polymineral concentrates. Full dating measurements were made using the same equipment but on HF-etched, 150–250 µm quartz fractions. Equivalent dose determinations were made on 16 aliquots per sample using an OSL SAR procedure [89]. We recognise that the number of aliquots measured was low; however, the laboratory profiles provide a further constraint on the distributions in equivalent dose. Equivalent dose distributions were assessed using a combination of statistical methods developed for luminescence dating and using Kernel Density Estimate and Abanico Plots (Figure 5). Dose rate estimates for these sediments were assessed using a combination of high-resolution gamma spectrometry (HRGS) and thick source beta counting (TSBC), which were reconciled with each other in a micro-dosimetric model, and attenuated for water content and grain size. The contribution from the cosmic dose was modelled after Prescott and Hutton [90].

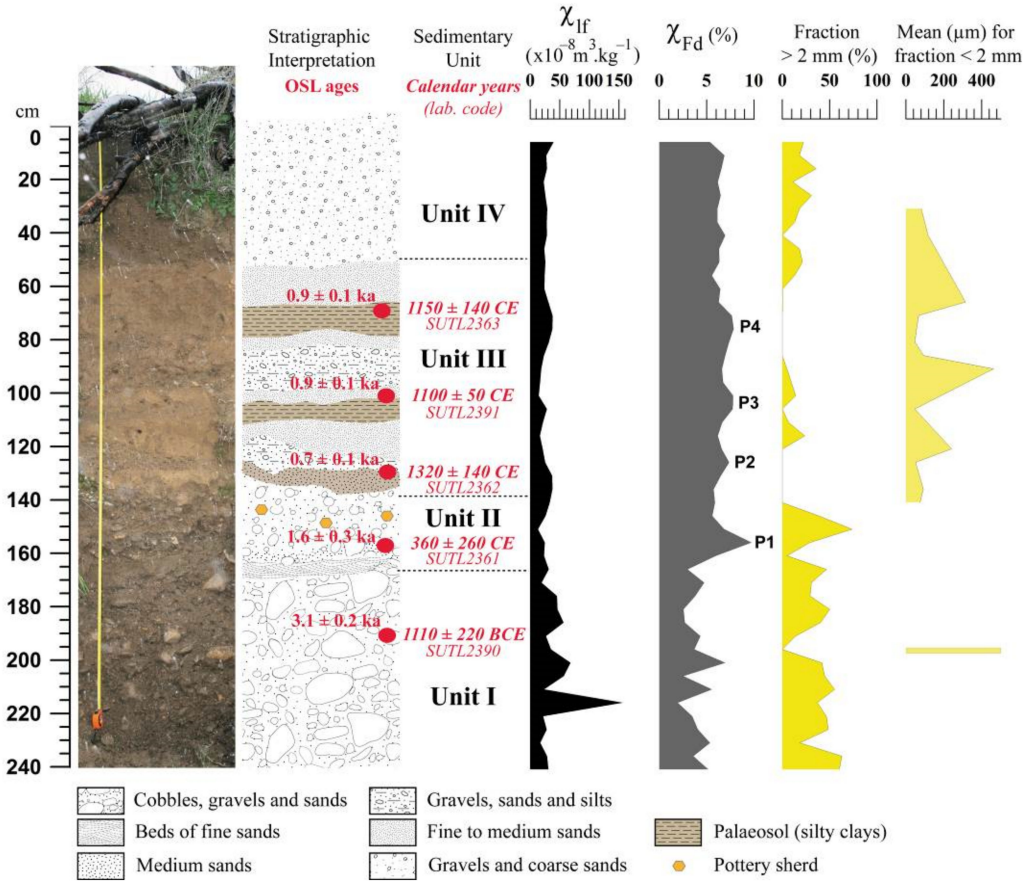

Figure 7. Stratigraphic profile studied at Pissonas. Red circles indicate the position of the OSL dating sample (lab. code is provided in Italics); Magnetic susceptibility (χ_{lf}) and Frequency Dependence (χ_{fd}) are expressed according to the depth; granuometry is given all along the profile using hand sieving method (yellow colour); and for the interval 130–30 cm using laser granulometry (light yellow colour).

4. Results

4.1. Lilas Sediment Profile Stratigraphy

Based on the magnetic parameters (magnetic susceptibility and frequency dependence) and granulometric analyses, four sedimentary units can be identified (Figure 7) and are described below:

Sedimentary Unit I/Terrace 3a (240–170 cm in profile) is situated at the base of the profile and is mostly composed of a mixture of large rounded cobbles and pebbles embedded within a coarse unconsolidated sandy matrix. On average, 40% of particles are coarser than 2 mm in size. Some intercalations of thin layers of sands mixed with small gravels are nevertheless observed at 2.30 and 1.95–1.90 m, thus indicating some periodicity to low energy deposition or rapid lateral migration of the streambed. Magnetic susceptibility measurements show the highest signal of all the profile acquired for Unit I from 2.15 to 1.75 m, where values range between 40 and 160 $\times$ $10^{-8}$$m^3$·$kg^{-1}$; the peak is reached at 2.15 m along the profile. A sample for OSL dating was taken from a thin layer of intercalated medium sands (SUTL2390). Frequency dependence was low in Unit I, with values generally in the range of 3 to 4%, with a single maximum at 7% (2.00 m). There was no evidence to suggest the development of a palaeosol in Unit I.

Sedimentary Unit II/Terrace T3b (170–140 cm in profile) is generally composed of coarse rounded pebbles embedded within a sandy matrix with no stratification. At the base of Unit II, there is a thin layer (10 cm) of fine-grained sediments that show some cross-bedded features. Above this, Unit II exhibits some similarities with Unit I in terms

of granulometry, except for the paucity of cobbles. A very broad grain-size distribution ranging from very large pebbles to sand-sized sediments suggests episodic changes in the energy of deposition. The presence of large rounded sherds of pluricentimetric size (orange colour; Figure 4b) is a new feature. Magnetic susceptibility values are lower than those observed in Unit I, ranging between 10 and 40 $\times 10^{-8} m^3 \cdot kg^{-1}$. There is more moderate fluvial activity towards the top of the unit, with the formation of a palaeosol at 1.60 cm, revealed by the presence of a high-frequency dependence, with values c. 10%. This palaeosol P1 was sampled for OSL dating (SUTL2361; Figure 7).

Sedimentary Unit III/Lower-Mid Terrace T2 (140–50 cm in profile) is composed of fine-grained sediments, ranging from fine silts to medium-coarse sands (500 µm), with two intercalations of gravels from 1.25 to 1.20 m and 0.95 to 0.80 m respectively. Compared to Units I and II, unit III shows stratification in the fine-grained layers identified at 1.25, 1.00, and 0.65 m, revealing constant and low energy of deposition. The magnetic susceptibility signal is similar to unit II, with values generally less than 40 $\times 10^{-8} m^3 \cdot kg^{-1}$, with minima at the gravel horizons (10 $\times 10^{-8} m^3 \cdot kg^{-1}$). Frequency dependence is relatively constant, oscillating between 7 to 8%, with maxima in the dark brown horizons (palaeosols P2, P3 and P4; Figure 7) composed of silty sands and fine sands (mean grain size is around 100 µm). Three samples were collected for OSL dating at 1.30, 1.00, and 0.70 m, from fine-grained horizons within Unit III (SUTL2362, SUTL2391, and SUTL2363; Figure 7 and Table 2).

Sedimentary Unit IV/Top of Terrace T2 (50–0 cm in profile) is the modern agricultural plough soil. It consists of homogeneous angular gravels (20% of the total of the sediments) embedded within a coarse sandy matrix. No sample was taken for OSL dating from this layer due to the heterogeneity of the sediments and the risk of reworked material due to modern agricultural plough. The magnetic susceptibility signal is lower than Unit III, showing values below 20 $\times 10^{-8} m^3 \cdot kg^{-1}$. Frequency dependence is a little lower than for Unit III, with values oscillating around 6%, revealing a modest contribution of superparamagnetic grains.

4.2. Magnetic Susceptibility Values of the Lilas Catchment Lithologies and Alluvial Sediments

Magnetic susceptibility measurements were conducted on both rock samples (hard lithology) and soft material (unconsolidated sediments) at the catchment scale of this study. Results are reported in Figure 8 and Table 3.

The bedrock lithology in the northern and eastern upper reaches of the Lilas catchment is characterised by a prevalence of metamorphic rocks (Figure 1), mainly composed of schists, phyllites, and marbles, and by limestone in the SE catchment. Magnetic susceptibility measurements were undertaken (sampling sites number 10, 11, and 12; Figure 8), and they generally exhibit a very low signal, generally centred around 10 $\times 10^{-8} m^3 \cdot kg^{-1}$, while the frequency dependence also reveals low values, situated around 1.5 and 3%, suggesting a relatively low contribution of the superparamagnetic particles. Neogene fluvio-lacustrine sediments characterising the Gides basin (sampling site number 6; Figure 8) exhibit a low signal of 10 $\times 10^{-8} m^3 \cdot kg^{-1}$, while χ_{fd} is about 5%. Mid-stream ophiolites in the area of Pissonas-Drako Spilio (sampling sites number 8 and 9; Figure 8) reveal a high χ_{lf} with values situated around 800 $\times 10^{-8} m^3 \cdot kg^{-1}$. The southern upper reaches were not investigated at this stage, but the presence of eruptive rocks in the eastern part of the Voudochi Mountain range could be associated with the reworking of magnetic particles eroded due to the incision of Lilas river tributaries (Figure 8).

Alluvial deposits (samples 1 to 5; Figure 8) were investigated along the main course of the Lilas river in order to evaluate the changes in terms of magnetic properties of both the present-day and inherited (alluvial terraces) sediments. In the Mistros area, three samples (numbered 1, 2, and 3 in Figure 8) of present-day river sediments reveal χ_{lf} values ranging from 10 to 40 $\times 10^{-8} m^3 \cdot kg^{-1}$ and χ_{fd} values oscillating from 3.5 to 5 $\times 10^{-8} m^3 \cdot kg^{-1}$. A similar signal is also reported for the upper stream area of Mistros (samples 4 and 5, Table 3 and Figure 8). In the area of Pournos, the presence of red soils (Terra Rossa;

sample number 7; Figure 8) that correspond to the alteration of Neogene fluvio-lacustrine deposits reveals high magnetic susceptibility values, around 250 $\times$ $10^{-8}m^3 \cdot kg^{-1}$ with a high contribution of superparamagnetic particles with χ_{fd} at about 13%. Results suggest that soft sediment, originating from the area composed of metamorphic and carbonate rocks, are enriched with ultra-fine magnetic particles when crossing the Gides basin.

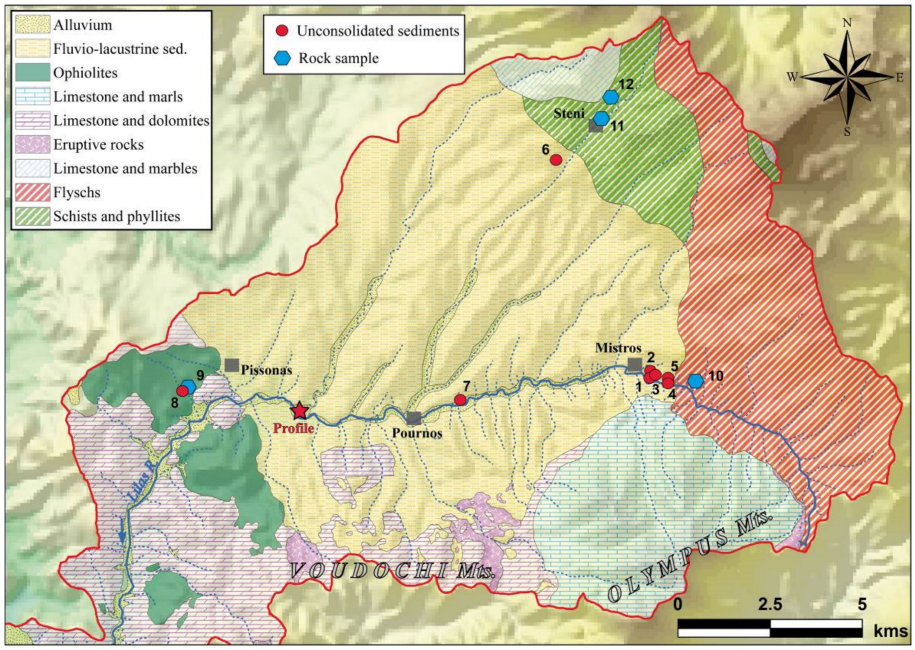

Figure 8. Location map of the samples studied for magnetic parameters with geology of the Lilas catchment. Grey squares: modern towns. The numbers refer to Table 3.

Table 3. Magnetic susceptibility results for samples coming from the Lilas catchment. Refer to Figure 7 for exact location of the sampling sites.

Material	Site Reference (Figure 7)	Area	Texture/Geology/Environment	χ_{lf} ($\times 10^{-8} m^3 \cdot kg^{-1}$)	χ_{fd} (%)
Unconsolidated sediments	1	Mistros (upper reaches)	Alluvial sands to gravels	11.6	4.2
	2	Mistros (upper reaches)	Alluvial sands	32.6	4.9
	3	Mistros (upper reaches)	Alluvial sands to gravels	42.9	3.7
	4	Mistros (upper reaches)	Sands to gravels (Alluvial terrace)	40.9	4.8
	5	Mistros (upper reaches)	Sands (Alluvial terrace)	28.4	6.3
	6	Steni (upper reaches)	Clays to fine sands	10.7	4.7
	7	Pournos (mid-stream)	Terra Rossa (red soils)	244.1	13.2
	8	Pissonas (mid-stream)	Oxidised clays and sands (above ophiolitic bedrock)	1071.2	1.5

Table 3. *Cont.*

Material	Site Reference (Figure 7)	Area	Texture/Geology/Environment	χ_{lf} ($\times 10^{-8} m^3 \cdot kg^{-1}$)	χ_{fd} (%)
Rock sample	9	Pissonas (mid-stream)	Ophiolite	793.6	1.1
	10	Mistros (upper reaches)	Flyschs	11.3	1.7
	11	Steni (upper reaches)	Phyllites	10.1	2.8
	12	Steni (upper reaches)	Limestone	11.3	2.1

4.3. Dating Results—Geochronology of Alluvial Units

Table 4 lists the buried doses and environmental dose rates for the Lilas terrace samples, together with the corresponding depositional ages.

Table 4. OSL dating results (calculated from 2011 CE).

Sample ID	Depth/cm	Dose Rate/mGy a^{-1}	Stored Dose/Gy	Age/ka	Age/Calendar Years	Sedimentary Unit (SU)/Terrace Level (Section 4.1)
2363	70	3.40 ± 0.12	2.9 ± 0.5	0.9 ± 0.1	1150 ± 140 CE	Top of SU III/Terrace T2
2391	100	2.61 ± 0.13	2.4 ± 0.1	0.9 ± 0.1	1100 ± 50 CE	Mid of SU III/Terrace T2
2362	130	2.59 ± 0.17	1.8 ± 0.4	0.7 ± 0.1	1320 ± 140 CE	Base of SU III/Terrace T2
2361	155	2.31 ± 0.21	3.8 ± 0.5	1.6 ± 0.3	360 ± 260 CE	Base of SU II/Terrace T3b
2390	190	2.05 ± 0.13	6.4 ± 0.2	3.1 ± 0.2	1110 ± 220 BCE	Top of SU I/Terrace T3a

Fluvial gravels, and associated fines, are apt to contain a mix of grains, some of which are well bleached at deposition and others that, under a cover of water, are poorly bleached at deposition (i.e., a response to the filtering and attenuation of the solar spectrum in water [91]). All samples showed some heterogeneity in the distribution of equivalent doses (Figure 9). For several samples, a number of aliquots returned normalised natural luminescence signals in excess of saturation, and these must indicate the aliquots that contain a mix of poorly bleached and unbleached material (some of which must have large residuals). With such sediments, the best estimate of the true burial dose might be considered to be the lowest measured dose or population of dose(s) [92–95]. Therefore, age estimates for these samples were determined from the weighted and robust means, varying between 6.4 ± 0.2 Gy and 1.8 ± 0.4 Gy.

The samples were also characterised by heterogeneity in radionuclide concentrations, with K concentrations in the range of 2.0 to 1.3%, U concentrations of 2.6 to 1.9%, and Th concentrations of 9.3 to 6.1 ppm. However, there was a strong correlation between the position in the stratigraphy and radionuclide concentration, with the samples at depth marked by lower concentrations (i.e., K 1.3%, U 1.8 ppm, Th 6.9 ppm) than the samples at height (i.e., K 1.9%, U 2.4 ppm, Th 9.3 ppm). Infinite matrix dose rates were calculated from these using the conversion factors of Sanderon [96] and adjusted for attenuation by grain size and chemical etching using the datasets of Aikten [97] and Bell and Zimmerman [98], respectively. These were reconciled with the measured beta doses (TSBC) rates and an estimate of the cosmic dose contribution in a dosimetric model to obtain total environmental dose rates. The total dose rates varied with position in the stratigraphy, with lower values at the base of the section, 2.1 mGy a^{-1} to higher values at the top, 3.4 mGy a^{-1}.

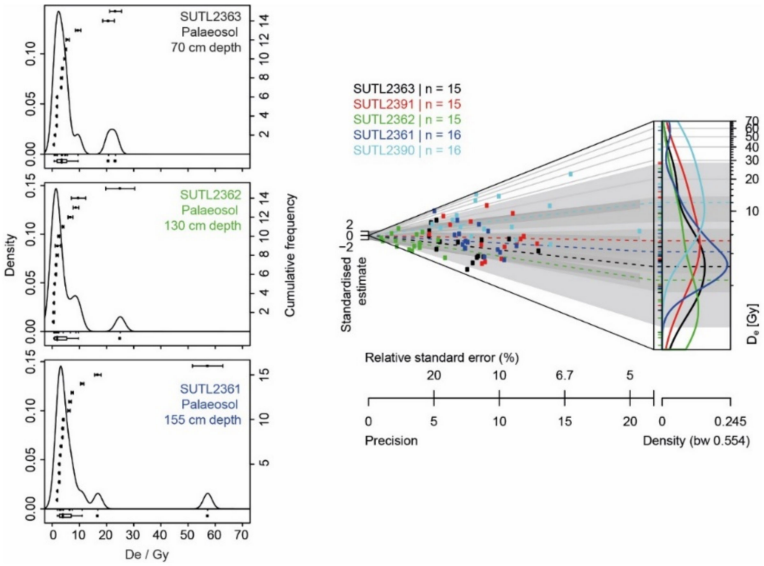

Figure 9. Equivalent dose distributions as Kernel Density Estimate (KDE) and Abanico plots for SUTL2361-2362-2363 (the palaeosols) and SUTL2390-2391 (the fluvial sands).

The burial doses of 6.4–1.8 Gy, together with dose rates of 2.1–3.4 mGy a^{-1}, correspond to depositional ages in the range of 3.1 ± 0.2 to 0.9 ± 0.1 ka. Depositional ages of 1.8 ± 0.3 ka (250 ± 280 CE), 0.7 ± 0.1 ka (1360 ± 130 CE) and 0.9 ± 0.1 ka (1150 ± 140 CE) were obtained for the palaeosol horizons identified on Figure 7. In calculating the above ages, in the absence of field gamma spectrometry, it was assumed that the environmental dose rate received at each full dating location was location-specific. In reality, the gamma dose rate received at any point in the sequence is the sum of the contributing gamma radiation from all horizons within a ~30 cm sphere of influence around that point. For example, the two lowermost palaeosol samples in the Lilas profile are separated by 25 cm, which contains a ~10 cm thick sandy gravel. An alternative estimate of the total gamma dose received by the sediment at SUTL2361 and 2362 would include an average of the gamma dose contributions from each sampling location, i.e., 2.31 ± 0.21 and 2.59 ± 0.17 mGya^{-1}, respectively. Substituting these dose rate estimates into the age calculations would produce alternative estimates of 1.6 ± 0.3 ka (360 ± 260 CE) and 0.7 ± 0.1 ka (1320 ± 140 CE; Figure 10).

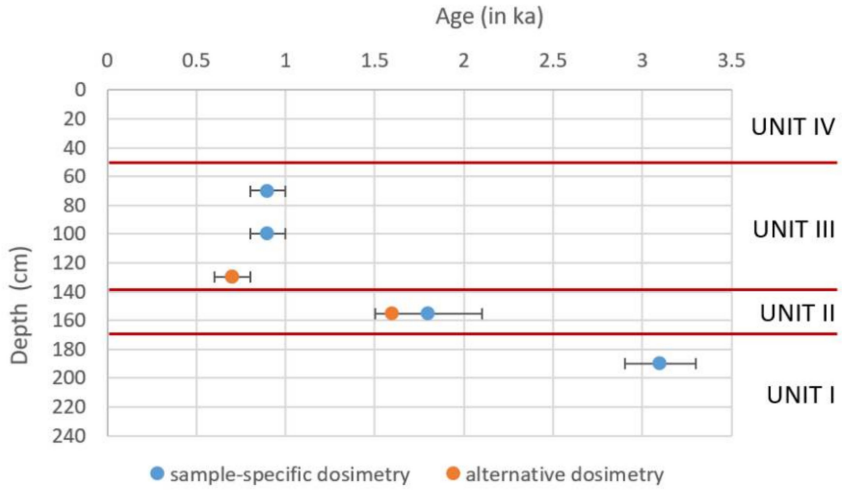

Figure 10. Age-depth profile for samples SUTL2361, 2362, 2363, 2390, and 2391 (see Table 4).

5. Discussion

5.1. Historical Alluviation of the Lilas River and Correlations with Regional Plaeofluvial Studies

In terms of chronostratigraphy, the Lilas river sequence spans the last three millennia and most probably the last 3500 years. The alluvial history recorded for the Lilas river shows obvious similarities with other regional records, in particular with Crete [19,20] and southern Euboea [24]. The following is a reconstruction of the history of the Lilas river catchment, combining the new evidence reported here with our regional studies:

The top of the coarse-grained sedimentary Unit I is dated to the 13th to the 9th centuries BCE. The sedimentary matrix exhibits high magnetic susceptibility values and low-frequency dependence. Together with coarse granulometry, this evidence suggests that a palaeosol is not developed in Unit I. As χ_{fd} is low, it rather suggests delivery of a specific source rich in magnetic minerals within the drainage basin. On this point, oxidised layers from the Neogene fluviolacustrine deposits of the Gides basin and eruptive rocks could provide magnetic particles. The northern slopes of the Voudochi mountain range were likely occupied in the Middle to Late Helladic periods—the sites have remained poorly known—but changes in regional land use, as previously forested land was turned to agriculture, likely led to increased erosion, especially as this coincided with a period of higher humid conditions. The alluviation that generated Unit I/terrace 3a can be interpreted as a regional phenomenon concerning the whole drainage basin, with erosion in the upper catchment of magnetic lithologies, during the second half of the second millennium BCE. Regarding the chronology of the terrace T3a formation, our results are in agreement with the lithostratigraphical data obtained in the Anapodaris gorge in Crete [19], where a thick and coarse-grained terrace formed between ca. 1400 and 1000 BCE.

It is also interesting to compare our results with other geoarchaeological data collected in the lower Lilas catchment and the surrounding drainage basins, where archaeological excavations also attest to a high detrital input during the late 2nd millennium BCE. First, the deltaic plain of the Lilas basin was investigated by coring during the late 2010s [31,32]; however, the chronostratigraphy did not record alluvial deposition between the late 2nd millennium BCE to the early 1st millennium BCE. The only inference from this study was the existence of a palaeochannel situated west of the present-day delta and dated to this period (Figure 11). Second, further along the coast, geoarchaeological evidence collected at Eretria (Figure 1) produced evidence for a phase of intensive alluviation that created a large deltaic plain at the beginning of the first millennium BCE. Indeed, core chronostratigraphy [31,99] revealed a detrital input from small drainage basins (<5 km^2) that delivered tremendous quantities of sediment to the coastal area compared to the size of the catchment [31]. This major sediment depositional phase was dated to the late 2nd millennium BCE and probably lasted several centuries [31,99]. In addition to the coring results, archaeological excavations conducted by the Swiss School of Archaeology in Greece since the 1960s at Eretria revealed the existence of a channelised stream flowing into the city that probably contributed, in part, to the artificial formation of the deltaic plain from the Geometric period onward (9th cent. CE [100]). A number of floods are recorded for the Early Iron Age [101,102]. During the Geometric period, the inhabitants of Eretria protected themselves against these floods by building walls around their houses [102]. Further regional evidence for high fluvial deposition at the beginning of the first millennium BCE is provided by the coastal sector of Amarynthos (Figure 1), where the Sarandapotamos river created a deltaic plain during the recent Holocene [31,103]. A major turn in the local environmental conditions is characterised by the transition from brackish to freshwater conditions, created by a new phase of deltaic progradation at the turn of the 1st millennium BCE. Again, there is evidence of alluvial deposition into the sea that correlates well with the evidence from Eretria and also with the dating of a massive phase of sediment aggradation recorded in the mid part of the Lilas basin.

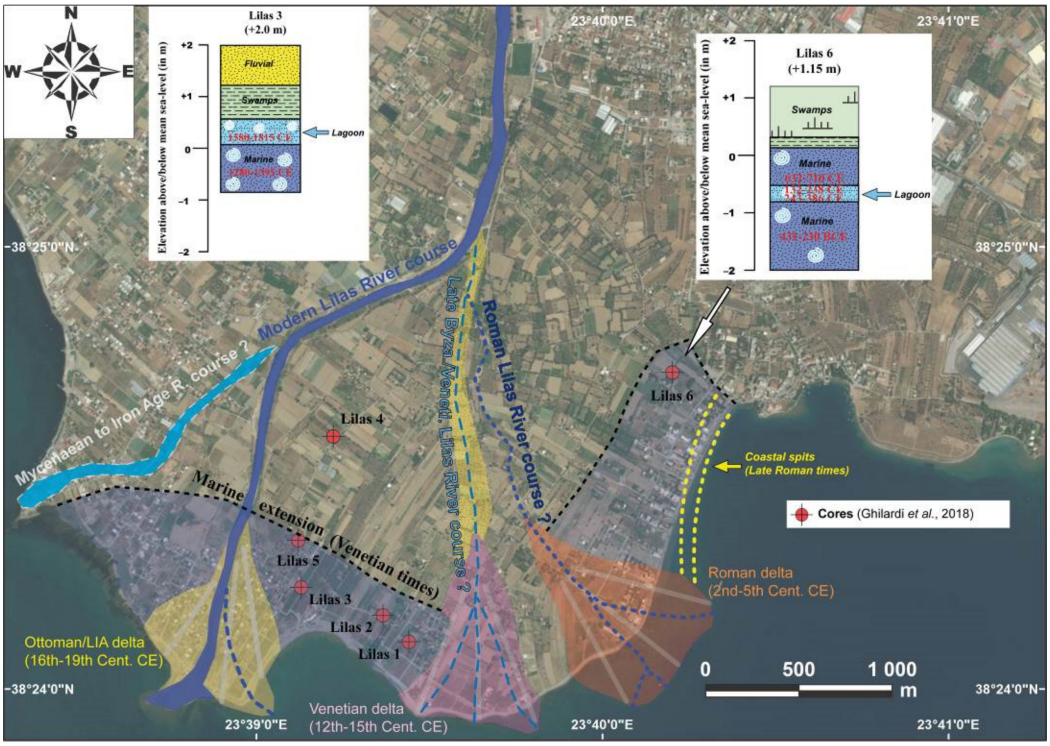

Figure 11. Palaeogeographical reconstructions of the Lilas river delta for the last three millennia (modified after [31]).

After a phase incision of Unit I, which roughly occurred around the mid-first millennium BCE, between the Archaic and Classical periods, we record a new phase of coarse-grained alluvial vertical accretion at Pissonas. Sedimentary Unit II contains archaeological material (pottery sherds of orange clay), unlike the Mycenaean terrace formation. The initial phase of deposition of this second phase of coarse alluvial material, characterised first by the development of a thin palaeosol (P1, Figure 7) as evidenced by a sharp peak in χ_{fd}, is dated from the 1st to the 5th cent. CE. To this point, in the deltaic plain of the Lilas river, sedimentary cores record evidence of a major phase of deltaic progradation (Figure 11 [31]) dated between the 2nd to the 4th cent. CE and which took place in the easternmost part of the deltaic plain. The marine redistribution of the fluvial sediments deposited into the sea created a series of coastal barriers that isolated a lagoon to the north [31]. A large part of this Roman delta has been cut off due to a long term coastal erosional process. The prodelta is that all remains, as seen in aerial photographs [31].

In comparison to other palaeofluvial research conducted in Euboea, the southernmost part of the island also experienced an important erosive crisis during Hellenistic to Roman times: in the Paximadhi peninsula (Figure 1), a thick accumulation of coarse-grained material has been dated using radiocarbon on organic remains embedded within the sedimentary matrix [24].

Following this deposition dated to Roman times, a new phase of incision is documented by a sharp transition in terms of granulometry: with sedimentary Units III and IV, characterised by finer-grained sedimentation and terrace T2 by intercalations of silty sands and coarse sands (Figure 3b). Therefore, the energy of deposition was generally lower after Roman times, also allowing the formation of at least three palaeosols (P2, P3, and P4; Figure 7) as indicated by the high-frequency dependence, suggesting phases of hydrological stability. The age of deposition of this ca. 1 m thick sedimentary unit is centred around 1100–1200 CE. The SAR OSL age estimates imply that the sediments were deposited relatively rapidly; the age constraints for the upper two palaeosols are within error of each other (Table 2), with a slight age reversal between the third palaeosol (likely an artefact

of the statistical calculation of burial dose on these fluvially influenced palaeosols). The nature of the samples—palaeosols (as confirmed by the magnetics results)—indicated that although the aggradation of the terrace deposits was rapid, it was punctuated by periods of stability sufficient to allow at least some soil formation between phases of significant alluviation. The range of sediments that have accumulated between SUTL 2362 and 2391 (c. 100–130 cm down profile) suggests further fluvial activity in the upper Lilas basin but with aggregate confined to gravels and coarse sands. This rapid phase of deposition, with a high sediment load, has been reported in the Lilas delta, with a new deltaic lobe created west of the Roman palaeodelta (Figure 11), related to the defluviation of the main river course westwards.

The last phase of alluvial aggradation is reported for Unit IV. This must date to the Ottoman period or later. It is noteworthy that the core chronostratigraphy for the present-day Lilas delta [31] reveals a massive alluvial deposition into the sea that probably occurred since the 16th century CE (Figure 11) and accelerated over the last 150 years [32]. Indeed, west of the Late Byzantine-Venetian delta, lateral migration of the Lilas river occurred, with the delta prograding over the last few centuries.

Following this, incision has been dominant, as the Lilas river has remained entrenched within its course, and delta progradation has been stable, with no significant retreat or advance.

5.2. On the Identification of Mycenaean and Roman Coarse-Grained Alluvial Terraces and on the Possible Mixed Climatic/Anthropogenic Origins

Since the work of C. Vita-Finzi [2], attempting to disentangle natural from anthropogenic origins of historical alluviation of Mediterranean rivers, this vibrant geoarchaeological topic has been a matter of controversial debate. In the case of the Lilas river, the formation of the historical alluvial terraces appears to be the result of a combination of fluvial dynamics, land use and fluctuating climatic conditions since at least the Mycenaean period (1600–1050 BCE).

For this last period, palaeofluvial research conducted in Crete revealed the existence of a so-called «Minoan Little Ice Age» [104], with a major aggradation phase of coarse material deposited around 1500 BCE in the river valleys. This phenomenon lasted until probably 1250 BCE [104]. This thick deposition is also reported and well-studied in south-central Crete for the Anapodaris river [19], where the initial stage of deposition of this coarse sedimentary unit is dated ca. 1400 BCE and lasted until 1000 BCE (Figure 12).

In order to elucidate the exact origins of the first coarse-grained alluvial deposition of the Lilas river during the Late Bronze Age, the effects of anthropogenic activities on land use must be considered. There is little archaeological evidence of land use from this period. Indicators for a fluctuating density of sites in terms of occupation are clear [47,48,105], but they are too scattered and scarce to retrieve any relevant information regarding land-use types.

The most reliable information for the estimation of historical land use can be obtained from regional palaeoecological studies, even if the precise spatial extent of pollen reconstructions obtained for a single core are difficult to estimate. The available pollen data for Euboea are restricted to the Amarynthos area [31], and for this, the archive is restricted to the Late Mycenaean/Geometric periods. This revealed that the dominant land cover was a clear open forest. Arboreal taxa are scarcely represented, with low percentages of *Pinus* and *Quercus* sp. [31]. Meanwhile, anthropogenic markers are visible with crop development (cereal pollen) together with pastoralism (coprophilous fungi *Sordaria* type) at the beginning of the 1st millennium BCE. There is no available pollen data in the Amarynthos sector for the later cultural periods due to the low preservation of pollen within medium-grained sediments (fluvial input of the Sarandapotamos river [31]) dated from the early 1st millennium BCE. Further afield, the proxy pollen records from Attica are informative about historical land use in the Vravron [72] and Marathon areas [106], respectively. For the Marathon site, the pollen sequence is not continuous, and the chronostratigraphy does not allow a reliable interpretation in terms of land use over the last three millennia. For the Vravron

site, the Late Bronze Age, and the Mycenaean period (1600–1050 BCE) in particular, are well documented and are characterised by an important agricultural development where cereal cultivation is central within an open forest landscape. As in Amarynthos, pine and oak forests are reduced in the area of Vravron (Figure 12), and for both sites, percentages of representation of arboreal taxa are the lowest in the pollen sequences, thus indicating that the soils might have been exposed to runoff and incision of the soft sediments. This vegetation pattern could be ascribed to the intensification of human activities during the Mycenaean settlement phase [106]. The wet (Figure 12 [36]) and cold [35] conditions that peaked around the 1st millennium BCE in the Aegean Sea are observed in a period of high land degradation with soil exposure due to a multi-centennial period of intensive land use. The combination of both parameters is undoubtedly responsible for the alluvial terrace formation during the Mycenaean times to the Early Iron Age in central-west Euboea Island. Further south, in Peloponnese, the Late Helladic (Mycenaean) is characterised by a dense settlement pattern associated with relative landscape stability. The detrital input reported for this period should be seen as the result of land-use strategies such as terracing [107,108]. Isolated short-term sedimentation events dating to the end of the Late Helladic period are recorded in the alluvial deposits of the Phlious Basin [18], at Tiryns in the Argive Plain, and at Chania and Mycenae [109–111]. These events may suggest lapsed maintenance after the breakdown of the Mycenaean palatial economy.

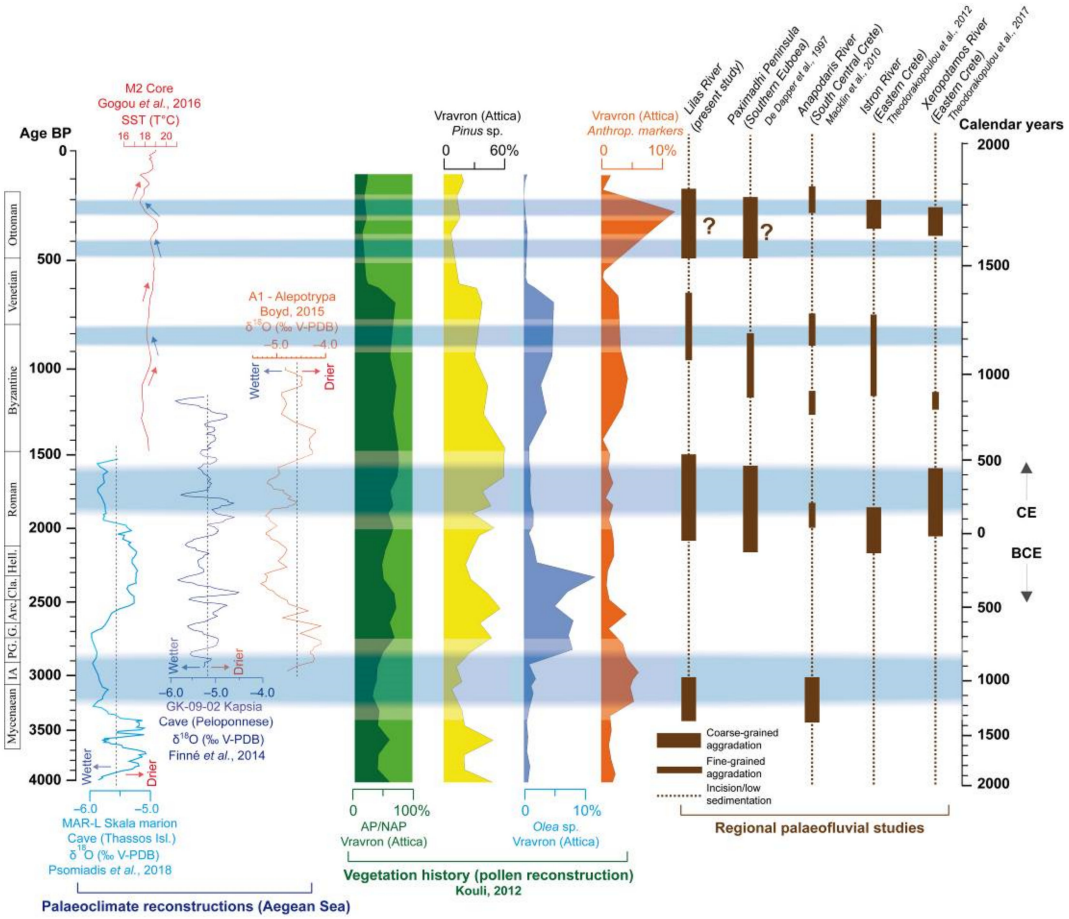

Figure 12. Palaeoclimatic reconstructions obtained for the Aegean Sea and Peloponnese (see Figure 1 for location of the different sites) vs. pollen results derived from the Vravron sequence (Figure 1 [72]) and palaeofluvial reconstructions obtained for islands of Euboea [24] and Crete [19–21]. Blue lines indicate wet episodes [33,36].

Above the Mycenaean phase of alluviation (Unit I), new coarse-grained sediment is dated from the first half of the first millennium CE (centred at 250 CE). The unit contained

re-deposited well-rounded fragments of ancient Greek pottery, thus complementing the OSL assay. The development of a thin palaeosol at the base of Unit II, as revealed by the high-frequency dependence, is probably indicative of agricultural practices in a context of a brief lower hydrosedimentary activity at the onset of the first millennium CE. Land-use information derived from the pollen sequence of Vravron indicates a slight decrease in *Olea* cultivation during Roman times and generally low agricultural practices while deciduous forests expanded under wet climatic conditions (Figure 12). This is also in accordance with the regional south Greece vegetation and land use pattern that shows, after the onset of the first millennium CE, an expansion of deciduous forest vegetation and a coeval retreat of both cultivations (*Olea*, cereals, *Juglans*) and pastoral activity indications [112]. It seems that despite a lower human density in the interior during Roman times, the Lilas river experienced severe floods that incised older fluvial material (presence of sherds in Unit II). As a consequence, climate conditions were probably the main driver of the alluviation in the Lilas basin during the Roman era. This assumption can be confirmed by the fact that south Euboea and Crete experienced similar floods during Roman times [19,20,24] (Figure 12). The general climate conditions of the Roman times are characterised by the WRO suggesting increasing precipitation and runoff in the whole Eastern Mediterranean.

5.3. A Late Byzantine (?) to Venetian Fine-Grained Phase of Deposition and Possible Alluvial Activity during the Little Ice Age

Units III and IV (Figure 7), corresponding to Terrace 2 (Table 1), were mostly deposited over the last millennium. Three OSL depositional ages were obtained for the lower, central and upper parts of Unit III, with similar ages in the range 1100–1200 CE. This information indicates a rapid vertical accretion of sediments in a short period of time. From a palaeoclimate perspective, this period corresponds to the Medieval Climate Anomaly recorded in regional palaeoclimatic archives [33]. As a direct consequence of the increase in precipitation, the Aegean particularly experienced enhanced fluvial activity within an insular context. For comparison, south-central Crete experienced several flood events at 1.13, 1.10, 0.85 and 0.70 ka BP [19], while for eastern Crete, a major alluviation phase occurred from 850 and 1250 CE in different low stream areas [20,21]. Other studies conducted on the Greek mainland document alluviation in Epirus around the 11th cent. CE [14] and enhance risk from slope failures in the Peloponnesus in the 12th–13th cent. CE [12]. Our study with a focus on the Lilas river was, therefore, in good agreement with other regional palaeofluvial studies that indicated the Medieval Climate Anomaly was a period of intense runoff and flooding in the Aegean. Again, proxy land use information available from the nearby pollen record from Vravron (Eastern Attica) indicates that the Late Byzantine period is characterised by an important phase of land use [72] in the context of demographic growth. In particular, cereal and olive cultivations are recorded together with grazing activity [72]. An increase in agricultural activity indicators (both cultivation and grazing) has also been evidenced in the regional pollen record for south Greece [112]. Increased signs of agricultural activities linked with soil erosion at 850 cal. CE are observed in the area of Messolonghi, west Greece [113]. However, archaeological evidence for sustained agriculture in Euboea during the Late Byzantine period is scarce; therefore, we cannot directly relate this last cultural period to the thick fine-grained sedimentary Unit III. After a short Frankish occupation following the 4th Crusade (1204 CE), Euboea became a possession of the Venetian Republic for approximately two and half centuries [53,114]. As a direct consequence, land improvement was undertaken: approximately 50 towers were built on the entire island (Figure 5a) during the Venetian occupation in areas with extensive fertile agricultural land [114] (Figure 12), and the late 15th-century census shows a dense network of villages relying exclusively on agriculture [56]. The Gides basin holds the highest concentration of towers [53]—six buildings are still standing in the landscape (Figure 5b)—suggesting that this area was intensively exploited and developed for agricultural purposes. The agricultural renewal of Euboea during the Venetian period was accompanied by the development of agricultural lands in fertile environments [114], together with an obvious

reduction in the vegetation cover. This combination of forest opening and cereal cultivation led to soil exposure within the context of particularly wet climatic conditions centred on the 12th cent. CE. Important runoff occurred and created an erosion into the fine Neogene fluviolacustrine material caused by local tributaries of the Lilas river, thus creating a rapid vertical accretion of finely-grained material deposited by local tributaries along the main river course.

Similar to the Mycenaean/Iron Age and the Roman periods, the Late Byzantine-Venetian period appears to be represented by sediment aggradation within the Lilas basin, favoured by the combination of particular wet climate conditions and enhanced land use (mostly operated during the Venetian times) when cereal cultivation was concentrated in the Gides basin.

Above Unit III, further detrital input is recorded at the top of the sequence, corresponding with sedimentary Unit IV. This follows the up-profile trend in the increase in granulometry observed in Unit III, culminating in the deposition of more homogenous gravels. No attempt was made to date Unit IV. However, based on its magnetic properties, its sedimentary source appears to be the same as Unit III. It was likely that Unit IV was deposited during the Little Ice Age, a period of important runoff and flooding reported for the whole Aegean and revealed by previous palaeofluvial [8,9,12,20,21,76] and paleoenvironmental studies [33,72,113,115].

5.4. How Can We Explain the Hiatus/Incision Phases Observed during Ancient Greek and Early Byzantine Times?

Two hiatuses, potentially reflecting incision of the alluvial terraces, are inferred based on the combination of OSL sediment chronology and sedimentological observations/analyses of the investigated profile. As currently constrained, these events are dated to the mid-first millennium BCE (from Archaic to Hellenistic periods) and from the second half of the first millennium CE (from Palaeochristian to Early Byzantine periods), respectively.

From the Archaic to the Hellenistic period, archaeological evidence suggested that human activity was concentrated around the large cities of Chalkis and Eretria and along the coast. The hinterland would have been cultivated/grazed, but it was believed that the interior was more scarcely occupied. The proxy environmental record from Vravron (Attica) showed that cereal cultivation was important in the Mycenaean period. However, we note an increase in forest cover (mainly the pine forest) and a change in terms of land use, with extensive *Olea* cultivation replacing cereal cultivation during Ancient Greek times [72]. Soil exposure was perhaps less important from the Archaic to Hellenistic periods due to major land-use changes and territorial re-organisation in the first centuries of the first millennium. During this period, palaeoclimate conditions were associated with a prolonged dry period both in the north [36] and the Aegean Sea [37]. Alluvial deposition was probably limited, and the Lilas river experienced a negative balance in terms of hydrosedimentary activity from Archaic to Hellenistic times.

Following the Roman period, a second hiatus, or phase of incision, may have occurred at the turn of the 2nd millennium CE, prior to the later phase of fine-grained aggradation dated from 1100 CE. From a palaeoclimatic perspective, the period following the Roman period is known as the Dark Ages Cold event (also called Bond 1 event [116]). This period, spanning the Early Christian and Early Byzantine periods, is marked by dry and cold conditions. The local vegetation cover was reduced, as evidenced in nearby Attica [70]. Simultaneously, pollen records indicate an increase in pine forests in the mountainous areas of eastern Attica [72] (Figure 12) and a reduction in agricultural activity linked to declining human activity in Attica, with *Olea* and cereal cultivations very limited (Figure 12). The situation in central Euboea is perhaps similar, characterised by lower population levels during the Early Christian and Early Byzantine times. This is also evidenced in the regional pollen record in south Greece [117], reflected in a drop in cultivation proxies and anthropogenic indicators.

During both hiatuses, particularly cold and dry climatic conditions prevailed in the Aegean. Vegetation cover increased, most notably in the uplands, with an expansion of pine forests. The hydrosedimentary response of the rivers, such as the Lilas river, is characterised by reduced transportation of eroded material linked to a phase of incision. This situation occurred during Archaic-Hellenistic times and the Palaeochristian-Early Byzantine periods, respectively.

6. Conclusions

The sedimentological analyses and magnetic susceptibility studies, in combination with the OSL sediment chronology, have helped to reconstruct the Late Holocene palaeofluvial history of the Lilas river at the catchment scale. Our approach compares the geochronology of the alluvial terraces (situated mid-stream) with the core chronostratigraphy documented downstream in the delta to evaluate temporal and spatial relationships from *source to river mouth*, and interpret the dynamics of sediment transport. One aim of the study was to evaluate the impacts of Late Holocene alluviation on the morphology across the catchment scale.

Our results indicate that the morphology in the Lilas catchment was influenced by Late Holocene climatic variability, as experienced throughout the Aegean. As a direct consequence, local tributary/hillslope sediment supply experienced variations both in the amplitude and the magnitude of floods: the last 1.5 ka were associated with low energy fluvial conditions, reflected in low accumulation rates (fine-grained material deposited under conditions of reduced flood competence); whereas the Mycenaean to Roman periods were characterised by high energy fluvial conditions, with pronounced sediment aggradation. Four distinct phases of sediment aggradation have been identified within the Lilas catchment: (i) two coarse-grained sedimentation phases dating from the Mycenaean/Early Iron Age and the Roman times, respectively; (ii) the third phase of sediment vertical accretion, rapid and fine-grained, dated from the Late Byzantine to Venetian periods. This coincides with an intensification in land cultivation within the Gides basin (as evidenced by the identification of palaeosols and based on the magnetic properties of the sediments); (iii) a late phase of vertical accretion linked to the deposition of fine-grained fluvial sequences, broadly dated to the Little Ice Age.

This temporal framework is similar to those reported elsewhere in the Aegean [19,20], for example, in both central and eastern Crete. Further, the phases of sediment accumulation identified in the Lilas catchment in Roman, Late Byzantine to Venetian and during the Little Ice Age are represented downstream, at the mouth of the river, with the formation of three deltaic lobes following the same chronological sequence [31]. In general, phases of aggradation recorded over the last three and half millennia generally coincide with wet climatic conditions reported in the North Aegean Sea; they are also associated with a regional reduction in forest vegetation, which is coeval with a pronounced land use characterised by the development of cereal cultivation.

Our study also highlights two phases of incision, or very low sediment accumulation, during periods of more arid conditions linked to less intense agricultural activities in the interior of the Lilas catchment. The first phase of incision likely occurred in the mid-first millennia BCE, corresponding to Ancient Greek times, and the second, in the second half of the first millennium CE, corresponding to the Byzantine period.

Our results show that local changes in land use in the interior of the island contributed to the increased frequency and magnitude of floods, already heightened due to Late Holocene climate variability. Further work needs to be undertaken to develop a high-resolution chronology for the Lilas catchment, the drainage of Euboea Island, and, more generally, the Aegean region. Palaeofluvial research in Greece remains scarce, and further research will only contribute to our understanding of historical and prehistorical alluvial dynamics within the Aegean. The Aegean islands, characterised by small catchments, permit detailed investigations from a *source to delta* sediment transfer study approach.

Author Contributions: Conceptualisation, M.G.; methodology, M.G. and T.K.; Field investigation, M.G., A.B., Y.C. and D.D.; data curation, M.G., T.K., S.F., A.B., D.S., Y.C, F.D. and D.D.; writing-original draft preparation, M.G., T.K., K.K., A.B. and S.F.; visualisation, M.G. and T.K.; project administration, M.G.; Funding: M.G. All authors have read and agreed to the published version of the manuscript.

Funding: Aix-Marseille University. Fonds Incitatifs de Recherche (2010–2011) directed by Matthieu Ghilardi (CNRS) and Christophe Morhange (Aix-Marseille University).

Institutional Review Board Statement: Not applicable.

Informed Consent Statement: Not applicable.

Data Availability Statement: The data can be found in reference [88].

Acknowledgments: IGME (Athens, Greece) is thanked for delivering the authorisation of fieldwork. The authors would like also to thank four anonymous reviewers and the editor who provided fruitful comments and suggestions of improvement of the present paper.

Conflicts of Interest: The authors declare no conflict of interest.

References

1. Fouache, E. *The Mediterranean World Environment and History*; Elsevier Masson: Paris, France, 2003; p. 488.
2. Vita-Finzi, C. *The Mediterranean Valleys: Geological Changes in Historical Times*; Cambridge University Press: Cambridge, UK, 1969; p. 140.
3. Lafrenière, G. *The Decline of Nature: Environmental History and the Western Worldview*; Academia Press: Cambridge, MA, USA, 2008; p. 457.
4. Bintliff, J.L. Natural Environment and Human Settlement in Prehistoric Greece Based on Original Fieldwork. *BAR Suppl. Ser.* **1977**, *28*, 734.
5. Bintliff, J.L. Time, Process and Catastrophism in the Study of Mediterranean Alluvial History: A Review. *World Archaeol.* **2002**, *33*, 417–435. [CrossRef]
6. Wagstaff, M. Buried Assumptions: Some Problems in the Interpretation of the "Younger Fill" Raised by Recent Data from Greece. *J. Archaeol. Sci.* **1981**, *8*, 247–264. [CrossRef]
7. Van Andel, T.H.; Zanger, E.; Demitrack, A. Land Use and Soil Erosion in Prehistoric and Historical Greece. *J. Field Archaeol.* **1990**, *17*, 379–396.
8. Lespez, L. Geomorphic Responses to Long-Term Land Use Changes in Eastern Macedonia (Greece). *Catena* **2003**, *51*, 181–208. [CrossRef]
9. Lespez, L. Les Dynamiques des Systèmes Fluviaux en Grèce du Nord au Cours des 7 Derniers Millénaires: Vers une Approche Multiscalaire des Interactions Nature/Société. *Géomorphol. Relief Processus Environ.* **2007**, *1*, 49–66.
10. Dufaure, J.J. La Terrasse Holocène d'Olympie et Ses Équivalents Méditerranéens. *Bull. Assoc. Géogr. Fr.* **1976**, *433–434*, 85–94. [CrossRef]
11. Fouache, E.; Gaki-Papanastassiou, K. Les Crues Brutales dans la Plaine d'Argos (Grèce): Une Contrainte à l'Aménagement, de l'Antiquité à Nos Jours. *Géomorphol. Relief Processus Environ.* **1997**, *3*, 313–324. [CrossRef]
12. Fouache, E. L'Alluvionnement Historique en Grèce Occidentale et au Péloponnèse: Géomorphologie, Archéologie et Histoire. *Bull. Corresp. Hell.* **1999**, *35*, 235.
13. Pope, R.J.J.; Wilkinson, K.N.; Millington, A.C. Human and Climatic Impact on Late Quaternary Deposition in the Sparta Basin Piedmont: Evidence from Alluvial Fan Systems. *Geoarchaeology* **2003**, *18*, 685–724. [CrossRef]
14. Lewin, J.; Macklin, M.J.; Woodward, J.C. Late Quaternary Fluvial Sedimentation in the Voidomatis Basin, Epirus, Northwest Greece. *Quat. Res.* **1991**, *35*, 103–115. [CrossRef]
15. Krahtopoulou, A. Holocene Alluvial History of Northern Pieria, Macedonia, Greece. In *Landscape and Land Use in Postglacial Greece*; Halstead, P., Frederick, C., Eds.; Sheffield Academic Press: Sheffield, UK, 2000; pp. 15–27.
16. Lespez, L.; Dalongeville, R.; Noirel-Schutz, C.; Suc, J.-P.; Koukouli-Chryssanthaki, H.; Treuil, R. Les Paléoenvironnements du Site Préhistorique de Dikili Tash (Macédoine Orientale, Grèce). *Bull. Corresp. Hell.* **2000**, *124*, 413–434. [CrossRef]
17. Lespez, L.; Glais, A.; López-Sáez, J.A.; Le Drezen, Y.; Tsirtsoni, Z.; Davidson, R.; Birée, L.; Malamidou, D. Middle Holocene Rapid Environmental Changes and Human Adaptation in Greece. *Quat. Res.* **2016**, *85*, 227–244. [CrossRef]
18. Fuchs, M. An Assessment of Human versus Climatic Impacts on Holocene Soil Erosion in NE Peloponnese, Greece. *Quat. Res.* **2007**, *67*, 349–356. [CrossRef]
19. Macklin, M.G.; Tooth, S.; Brewer, P.A.; Noble, P.L.; Duller, G.A.T. Holocene Flooding and River Development in a Mediterranean Steepland Catchment: The Anapodaris Gorge, South Central Crete, Greece. *Glob. Planet. Change* **2010**, *70*, 35–52. [CrossRef]
20. Theodorakopoulou, K.; Pavlopoulos, K.; Athanassas, K.; Zacharias, N.; Bassiakos, Y. Sedimentological Response to Holocene Climate Events in the Istron Area, Gulf of Mirabello, NE Crete. *Quat. Int.* **2012**, *266*, 62–73. [CrossRef]
21. Theodorakopoulou, K.; Bassiakos, Y. Georchaeological Studies at the Cemetery of Ancient Kamara, Assisted by Optically Stimulated Luminescence (OSL) Dating: Insights in the Post-roman Hydrological Record of Eastern Crete. *J. Archaeol. Sci. Rep.* **2017**, *12*, 794–804.

22. Genre, C. Les Alluvionnements Historiques en Eubée, Grèce. Caractères Principaux, Chronologie, Signification. *Études Méditerr.* **1988**, *12*, 229–258.
23. Genre, C. Néotectonique et Développement des Terrasses de l'Holocène Récent: L'Exemple de l'Eubée (Grèce Centre Orientale). *Géomorphol. Relief Processus Environ.* **1999**, *5*, 143–158. [CrossRef]
24. De Dapper, M.; De Vliegher, B.M.; Peña Monne, J.L. Geoarchaeological Study of Historical Accumulations on the Paximadhi Peninsula (South Euboia, Greece). In *Geoarchaeology in Tropical and Mediterranean Regions*; Alexandre, J., De Dapper, M., Eds.; Académie Royale des Sciences d'Outre-Mer: Brussels, Belgium, 1997; pp. 91–107.
25. Wallinga, J. Optically Stimulated Luminescence Dating of Fluvial Deposits: A Review. *Boreas* **2002**, *31*, 303–322. [CrossRef]
26. De Long, S.B.; Arnold, L.J. Dating Alluvial Deposits with Optically Stimulated Luminescence, AMS 14C and Cosmogenic Techniques, Western Transverse Ranges, California, USA. *Quat. Geochronol.* **2007**, *2*, 129–136. [CrossRef]
27. Rittenour, T. Luminescence Dating of Fluvial Deposits: Applications to Geomorphic, Palaeoseismic and Archaeological Research. *Boreas* **2008**, *37*, 613–635. [CrossRef]
28. Cordier, S. Optically Stimulated Luminescence Dating: Procedures and Applications to Geomorphological Research in France. *Géomorphol. Relief Processus Environ.* **2010**, *16*, 21–40. [CrossRef]
29. Wallinga, J.; Bos, I.J. Optical Dating of Fluvio-Deltaic Clastic Lake-Fill Sediments—A Feasibility Study in the Holocene Rhine Delta (Western Netherlands). *Quat. Geochronol.* **2010**, *5*, 602–610. [CrossRef]
30. Genre, C. *Cartes des Linéaments Structuraux Établies à Partir des Images Landstat II et des Données Sismotectoniques OASP et IGME*; Research Report; CIEM: Poitiers, France, 1985; p. 12.
31. Ghilardi, M.; Vacchi, M.; Currás, A.; Müller Celka, S.; Theurillat, T.; Lemos, I.; Pavlopoulos, K. Géoarchéologie des Paysages Littoraux le Long du Golfe Sud-Eubéen (île d'Eubée, Grèce) au Cours de l'Holocène. *Quaternaire* **2018**, *29*, 95–120. [CrossRef]
32. Karymbalis, E.; Valkanou, K.; Tsodoulos, I.; Iliopoulos, G.; Tsanakas, K.; Batzakis, V.; Tsironis, G.; Gallousi, C.; Stamoulis, K.; Ioannides, K. Geomorphic Evolution of the Lilas River Fan Delta (Central Evia Island, Greece). *Geosciences* **2018**, *8*, 361. [CrossRef]
33. Gogou, A.; Triantaphyllou, M.; Xoplaki, E.; Izdebski, A.; Parinos, C.; Dimiza, M.D.; Bouloubassi, I.; Luterbacher, J.; Kouli, K.; Martrat, B.; et al. Climate Variability and Socio-Environmental Changes in the Northern Aegean (NE Mediterranean) during the Last 1500 Years. *Quat. Sci. Rev.* **2016**, *136*, 209–228. [CrossRef]
34. Xoplaki, E.; Fleitmann, D.; Luterbacher, J.; Wagner, S.; Haldon, J.F.; Zorita, E.; Telelis, I.; Toreti, A.; Izdebski, A. The Medieval Climate Anomaly and Byzantinum: A Review of the Evidence on Climatic Fluctuations, Economic Performance and Societal Change. *Qutaernary Sci. Rev.* **2016**, *136*, 229–252. [CrossRef]
35. Rohling, E.J.; Mayewski, P.; Abu-Zied, R.; Crasford, J.S.L. Holocene Atmosphere-Ocean Interactions: Records from Greenland and the Aegean Sea. *Clim. Dyn.* **2002**, *18*, 587–593.
36. Psomiadis, D.; Dotsika, E.; Albanakis, K.; Galheb, M.; Hillaire-Marcel, C. Speleothem Record of Climatic Changes in the Northern Aegean Region (Greece) From the Bronze Age to the Collapse of the Roman Empire. *Palaeogeogr. Palaeoclimatol. Palaeoecol.* **2018**, *489*, 272–283. [CrossRef]
37. Finné, M.; Bar-Matthews, M.; Holmgren, K.; Sundqvist, H.S.; Liakopoulos, I.; Zhang, Q. Speleothem Evidence for Late Holocene Climate Variability and Floods in Southern Greece. *Quat. Res.* **2014**, *81*, 213–227. [CrossRef]
38. Boyd, M. Speleothem from Warm Climates-Holocene Records from the Caribbean and Mediterranean Regions. Ph.D. Thesis, Department of Physical Geography, University of Stockholm, Stockholm, Sweden, 2015; p. 82.
39. Stiros, S.C.; Arnold, M.; Pirazzoli, P.A.; Laborel, J.; Laborel, F.; Papageorgiou, S. Historical Coseismic Uplift on Euboea island, Greece. *Earth Planet. Sci. Lett.* **1992**, *108*, 109–117. [CrossRef]
40. Pavlopoulos, K.; Kapsimalis, V.; Theodorakopoulou, K.; Panagiotopoulos, I.P. Vertical Displacements in the Aegean Coastal Zone (NE Mediterranean) during the Holocene Assessed by Geo-Archaeological Data. *Holocene* **2011**, *22*, 717–728. [CrossRef]
41. Evelpidou, N.; Vassilopoulos, A.; Pirazzoli, A. Holocene Emergence in Euboea Island (Greece). *Mar. Geol.* **2012**, *295–298*, 14–19. [CrossRef]
42. Drakopoulos, I.; Makropoulos, K.; Stavrakakis, G. *Junction of Evia–Beotia and Chalkida Diversion. Seismological Study*; Report for the Greek Ministry of Public Works; Greek Ministry of Public Works: Athens, Greek, 1984; p. 58. (In Greek)
43. Galanopoulos, A. Σεισμική γεωγραφία της Ελλάδος. *Ann. Géol. Pays Hell.* **1995**, *VI*, 83–121.
44. Papazachos, B.; Papazachou, C. *The Earthquakes of Greece*; Ziti Publisher: Thessaloniki, Greece, 1997; p. 304.
45. Gaki-Papanastassiou, K.; Cundy, A.B.; Maroukian, H. Fluvial versus Tectonic Controls on the Late Holocene Geomorphic and Sedimentary Evolution of a Small Mediterranean Fan Delta System. *J. Geol.* **2011**, *119*, 221–234. [CrossRef]
46. Kalamara, P.; Kosma, M.; Boukaras, K.; Chairetakis, Y. *The City of Chalkis*; Ministry of Culture and sports; Kapon: Athens, Greece, 2015; pp. 30–51.
47. Lemos, I.S. *The ProtoGeometric Aegean. The archaeology of the Late Eleventh and Tenth Centuries BC.*; Oxford University Press: Oxford, UK, 2002; p. 245.
48. Knodell, A.R. A Conduit Between Two Worlds: Geography and Connectivity in the Euboean Gulf. In *An Island Between Two Worlds: The Archaeology of Euboea from Prehistoric to Byzantine Times, Proceedings of International Conference, Eretria, Greece, 12–14 July 2013*; Tankosic, Z., Mavridis, F., Kosma, M., Eds.; Norwegian Institute at Athens: Athens, Greece, 2017; pp. 195–213.
49. Fachard, S.; Verdan, S. Chalkis and Eretria. In *The Oxford History of the Archaic Greek World*; Cartledge, P., Christesen, P., Eds.; Oxford University Press: Oxford, UK, 2022; Forthcoming.

50. Sackett, L.H.; Howell, R.J.; Jacobsen, T.W.; Popham, M.R. Prehistoric Euboea: Contributions toward a Survey. *ABSA* **1966**, *61*, 33–112. [CrossRef]
51. Fachard, S. *La Défense du Territoire d'Erétrie: Etude de la Chora et de ses Gortifications*; Infolio, Eretria, 21; Ecole Suisse d'Archéologie en Grèce: Gollion, Switzerland, 2012; p. 358.
52. Bakhuizen, S.C. *Studies in the Topography of Chalcis on Euboea*; Studies of the Dutch Archaeological and Historical Studies; E.J. Brill Publisher: Leiden, The Netherlands, 1985; Volume 11, p. 183.
53. Loizou, C. The Medieval Towers in the Landscape of Euboea: Landmarks of Feudalism. *J. Greek Archaeol.* **2016**, *1*, 331–352.
54. Koder, J. *Negroponte. Untersuchungen zur Topographie und Siedlungsgeschichte der Insel Euboia während der Zeit der Venezianerherrschaft*; Verlag der Österreichischen Akadamie der Wissenschaften: Vienna, Austria, 1973; p. 191.
55. Lock, P. The Towers of Euboea: Lombard or Venetian, Agrarian or Strategic. In *The Archaeology of Medieval Greece*; Lock, P., Sanders, G.D.R., Eds.; Oxbow: Oxford, UK, 1996; pp. 107–126.
56. Balta, E. *L'Eubée à la Fin du XVe Siècle. Economie et Population. Les Registres de l'Année 1474*; Association des Études d'Eubée: Athens, Greece, 1989; p. 448.
57. Kiel, M. The Turkish Aqueduct of Chalkis. In *Studies of the Dutch Archaeological and Historical Studies*; E.J. Brill Publisher: Leide, The Netherlands, 1985; Volume 11, pp. 151–157.
58. Luterbacher, J.; García-Herrera, R.; Akcer-On, S.; Allan, R.; Alvarez-Castro, M.C.; Benito, G.; Booth, J.; Büntgen, U.; Cagatay, N.; Colombaroli, D.; et al. A Review of 2000 Years of Paleoclimatic Evidence in the Mediterranean. In *The Climate of the Mediterranean Region*; Elsevier: Amsterdam, The Netherlands, 2012; pp. 87–185.
59. Finné, M.; Woodbridge, J.; Labuhn, I.; Roberts, C.N. Holocene Hydro-Climatic Variability in the Mediterranean: A Synthetic Multi-Proxy Reconstruction. *Holocene* **2019**, *29*, 847–863. [CrossRef]
60. Rohling, E.J.; Marino, G.; Grant, K.M.; Mayewski, P.A.; Weninger, B. A Model for Archaeologically Relevant Holocene Climate Impacts in the Aegean-Levantine Region (Easternmost Mediterranean). *Quat. Sci. Rev.* **2019**, *208*, 38–53. [CrossRef]
61. Kuhnt, T.; Schmiedl, G.; Ehrmann, W.; Hamann, Y.; Hemleben, C. Deep-Sea Ecosystem Variability of the Aegean Sea during the past 22 Kyr as Revealed by Benthic Foraminifera. *Mar. Micropaleontol.* **2007**, *64*, 141–162. [CrossRef]
62. Griggs, C.; De Gaetano, A.; Kuniholm, P.; Newton, M. A Regional High-Frequency Reconstruction of Mayejune Precipitation in the North Aegean from Oak Tree Rings, AD 1089–1989. *Int. J. Climatol.* **2007**, *27*, 1075–1089. [CrossRef]
63. Kotthoff, U.; Müller, U.C.; Pross, J.; Schmiedl, G.; Lawson, I.T.; Van De Schootbrugge, B.; Schulz, H. Lateglacial and Holocene Vegetation Dynamics in the Aegean Region: An Integrated View Based on Pollen Data from Marine and Terrestrial Archives. *Holocene* **2008**, *18*, 1019–1032. [CrossRef]
64. Finné, M.; Holmgren, K.; Shen, C.C.; Hu, H.M.; Boyd, M.; Stocker, S. Late Bronze Age Climate Change and the Destruction of the Mycenaean Palace of Nestor at Pylos. *PLoS ONE* **2017**, *12*, e0189447. [CrossRef]
65. Heymann, C.; Nelle, O.; Dörfler, W.; Zagana, H.; Nowaczyk, N.; Xue, J.; Unkel, I. Late Glacial to Mid-Holocene Palaeoclimate Development of Southern Greece Inferred from the Sediment Sequence of Lake Stymphalia (NE-Peloponnese). *Quat. Int.* **2013**, *302*, 42–60. [CrossRef]
66. Norström, E.; Katrantsiotis, C.; Finné, M.; Risberg, J. Biomarker Hydrogen Isotope Composition (δD) as Proxy for Holocene Hydroclimatic Change and Seismic Activity in SW Peloponnese, Greece. *J. Quat. Sci.* **2018**, *33*, 563–574. [CrossRef]
67. Unkel, I.; Schimmelmann, A.; Shriner, C.; Forsén, J.; Heymann, C.; Brückner, H. The Environmental History of the Last 6500 Years in the Asea Valley (Peloponnese, Greece) And Its Linkage to the Local Archaeological Record. *Z Für Geomorphol.* **2014**, *58*, 89–107. [CrossRef]
68. Bar-Matthews, M.; Ayalon, A.; Kaufman, A. Middle to Late Holocene (6500 years period) Paleoclimate in the Eastern Mediterranean Region from Stable Isotopic Composition of Spe-Leothems from Soreq Cave, Israel. In *Water, Environment and Society in Times of Climatic Change*; Issar, A.S., Brown, N., Eds.; Kluwer: Amsterdam, The Netherlands, 1998; pp. 203–214.
69. Bar-Matthews, M.; Ayalon, A.; Gilmour, M.; Matthews, A.; Hawkesworth, C.J. Sea–Land Oxygen Isotopic Relationships from Planktonic Foraminifera and Speleothems in the Eastern Mediterranean Region and Their Implication for Paleorainfall during Interglacial Intervals. *Geochim. Cosmochim. Acta* **2003**, *67*, 3181–3199. [CrossRef]
70. Triantaphyllou, M.; Kouli, K.; Tsourou, T.; Koukousioura, O.; Pavlopoulos, K.; Dermitzakis, M.D. Palaeoenvironmental Changes since 3000 BC in the Coastal Marsh of Vravron (Attica, SE Greece). *Quat. Int.* **2010**, *216*, 14–22. [CrossRef]
71. Ghilardi, M.; Revelles, J.; Glais, A.; Theodorakopoulou, K.; Theodoropoulou, T.; Lespez, L.; Longo, F.; Rossi, A.; Bellier, O.; Benedetti, L. Reconstructing Human-Environment Interactions in the Western Messara Plain (Phaistos, Crete, Greece) From the Emergence of City States to Byzantine Times. *J. Archaeol. Sci. Rep.* **2019**, *26*, 101909. [CrossRef]
72. Kouli, K. Vegetation Development and Human Activities in Attiki (SE Greece) During the Last 5000 Years. *Veg. Hist. Archaeobotany* **2012**, *21*, 267–278. [CrossRef]
73. Bintliff, J.L. Landscape Change in Classical Greece: A Review. In *Geoarchaeology of the Landscapes of Classical Antiquity*; Vermeulen, F., De Dapper, M., Eds.; Peeters: Leuven, Belgium, 2000; pp. 49–70.
74. Ehrmann, W.; Schmiedl, G.; Hamann, Y.; Kuhnt, T.; Hemleben, C.; Siebel, W. Clay Minerals in Lateglacial and Holocene Sediments of the Northern and Southern Aegean Sea. *Palaeogeogr. Palaeoclimatol. Palaeoecol.* **2007**, *249*, 36–57. [CrossRef]
75. Orland, I.J.; Bar-Matthews, M.; Kita, N.T.; Ayalon, A.; Matthews, A.; Valley, J.W. Climate Deterioration in the Eastern Mediterranean as Revealed by Ion Microprobe Analysis of a Speleothem That Grew from 2.2 to 0.9 ka in Soreq Cave, Israel. *Quat. Res.* **2009**, *71*, 27–35. [CrossRef]

76. Fouache, E. Un Exemple de Crise d'Alluvionnement Historique: La Terrasse d'Olympie. In *Le Commentaire de Paysages en Géographie Physique*; Mercier, D., Ed.; SEJER, Armand Colin, Collection U-Géographie: Paris, France, 2004; p. 256.
77. Cook, B.I.; Anchukaitis, K.J.; Touchan, R.; Meko, D.M.; Cook, E.R. Spatiotemporal Drought Variability in the Mediterranean over the Last 900 Years. *J. Geophys. Res.* **2016**, *121*, 2060–2074. [CrossRef] [PubMed]
78. Maher, B.A.; Taylor, R.M. Formation of Ultrafine-Grained Magnetite in Soils. *Nature* **1988**, *336*, 368–370. [CrossRef]
79. Dearing, J.A.; Dann, R.J.L.; Hay, K.; Lees, J.A.; Loveland, P.J.; Maher, B.A.; O'Grady, K. Frequency-Dependent Susceptibility Measurements of Environmental Materials. *Geophys. J. Int.* **1996**, *124*, 228–240. [CrossRef]
80. Ghilardi, M.; Kunesch, S.; Styllas, M.; Fouache, E. Reconstruction of Mid-Holocene Sedimentary Environments in the Central Part of the Thes-Saloniki Plain (Greece), Based on Microfaunal Identification, Magnetic Susceptibility and Grain-Size Analyses. *Geomorphology* **2008**, *97*, 617–630. [CrossRef]
81. Ghilardi, M.; Cordier, S.; Carozza, J.M.; Psomiadis, D.; Guilaine, J.; Demory, F.; Delanghe-Sabatier, D.; Zomeni, Z.; Vella, M.A.; Bony, G.; et al. The Holocene Fluvial History of the Tremithos River (South Central Cyprus) And Its Linkage to Archaeological Records. *Environ. Archaeol. J. Hum. Palaeoecol.* **2015**, *20*, 184–201. [CrossRef]
82. Ghilardi, M.; Delanghe, D.; Demory, F.; Leandri, F.; Pêche-Quilichini, K.; Vacchi, M.; Vella, M.A.; Rossi, V.; Robresco, S. Enregistrements d'Événements Extrêmes et Évolution des Paysages dans les Basses Vallées Fluviales du Taravo et du Sagone (Corse Occidentale, France) au Cours de l'Âge du Bronze Moyen à Final: Une Perspective Géoarchéologique. *Géomorphol. Relief Processus Environ.* **2017**, *23*, 15–35. [CrossRef]
83. Buurman, P.; Pape, T.; Muggler, C.C. Laser Grain-Size Determination in Soil Genetic Studies: Practical Problems. *Soil Sci.* **1996**, *162*, 211–218. [CrossRef]
84. Buurman, P.; de Boer, K.; Pape, T. Laser Diffraction grain-size characteristics of Andisols in perhumid Costa Rica: The aggregate size of allophane. *Geoderma* **1997**, *78*, 71–91. [CrossRef]
85. Blott, S.J.; Pye, K. Gradistat: A Grain Size Distribution and Statistics Package for the Analysis of Unconsolidated Sediments. *Earth Surf. Processes Landf.* **2001**, *26*, 1237–1248. [CrossRef]
86. Burbidge, C.I.; Sanderson, D.C.W.; Housley, R.A.; Allsworth Jones, P. Survey of Palaeolithic Sites by Luminescence Profiling, a Case Study from Eastern Europe. *Quat. Geochronol.* **2007**, *2*, 296–302. [CrossRef]
87. Kinnaird, T.C.; Sanderson, D.C.W.; Bigelow, G.F. Feldspar SARA IRSL Dating of Very Low Dose Rate Aeolian Sediments from Sandwick South, Unst, Shetland. *Quat. Geochronol.* **2015**, *30*, 168–174. [CrossRef]
88. Kinnaird, T.C.; Sanderson, D.C.W.; Bickett, A. *OSL Dating of Fluvial Terrace Deposits, Eubeoa, Greece*; Unpublished Report; University of Glasgow: Glasgow, UK, 2011.
89. Murray, A.S.; Wintle, A.G. Luminescence Dating of Quartz Using an Improved Single-Aliquot Regenerative-Dose Protocol. *Radiat. Meas.* **2000**, *32*, 57–73. [CrossRef]
90. Prescott, J.R.; Hutton, J.T. Cosmic Ray Contributions to Dose Rates for Luminescence and ESR Dating: Large Depths and Long-Term Time Variations. *Radiat. Meas.* **1994**, *23*, 497–500. [CrossRef]
91. Sanderson, D.C.W.; Bishop, P.; Stark, M.; Alexander, S.; Penny, D. Luminescence Dating of Canal Sediments from Angkor Borei, Mekong Delta, Southern Cambodia. *Quat. Geochronol.* **2007**, *2*, 322–329. [CrossRef]
92. Fuchs, M.; Lang, A. OSL Dating of Coarse-Grain Fluvial Quartz Using Single-Aliquot Protocols on Sediments from NE Peloponnese, Greece. *Quat. Sci. Rev.* **2001**, *20*, 783–787. [CrossRef]
93. Lepper, K.; Larsen, N.A.; McKeever, S.W.S. Equivalent Dose Distribution Analysis of Holocene Eolian and Fluvial Quartz Sandsequivalent Dose Distribution Analysis of Holocene Eolian and Fluvial Quartz Sands from Central Oklahoma. *Radiat. Meas.* **2000**, *32*, 603–608. [CrossRef]
94. Olley, J.M.; Caitcheon, G.G.; Murray, A.S. The Distribution of Apparent Dose as Determined by Optically Stimulated Luminescence in Small Aliquots of Fluvial Quartz: Implications for Dating Young Sediment. *Quat. Geochronol.* **1998**, *17*, 1033–1040.
95. Olley, J.M.; Caitcheon, G.G.; Roberts, R.G. The Origin of Dose Distributions in Fluvial Sediments, and the Prospect of Dating Single Grains from Fluvial Deposits Using Optically Stimulated Luminescence. *Radiat. Meas.* **1999**, *30*, 207–217. [CrossRef]
96. Sanderson, D.C.W. Thermoluminescence Dating of Vitrified Scottish Forts. Ph.D. Thesis, Paisley College, Paisley, UK, 1987.
97. Aitken, M.J. Dose Rate Data in SI Units. *PACT* **1983**, *9*, 69–73.
98. Bell, W.T.; Zimmerman, D.W. The Effect of HF Acid Etching on the Morphology of Quartz Inclusions for Thermoluminscence Dating. *Archaeometry* **1978**, *20*, 63–65. [CrossRef]
99. Ghilardi, M.; Psomiadis, D.; Pavlopoulos, K.; Müller-Celka, S.; Fachard, S.; Theurillat, T.; Verdan, S.; Knodell, A.; Theodoropoulou, T.; Bicket, A.; et al. Mid- to Late Holocene Shoreline Reconstruction and Human Occupation in Ancient Eretria (South Central Euboea, Greece). *Geomorphology* **2014**, *208*, 225–237. [CrossRef]
100. Krause, K. Naissance et Formation d'une Ville. *Hist. Archéol. Doss.* **1985**, *94*, 17–25.
101. Fachard, S.; Theurillat, T.; Psalti, A.; Ackermann, D.; Knoepfler, D. La Nécropole du Canal à Érétrie: Topographie et Inscriptions. *Bull. Corresp. Hell.* **2017**, *141*, 141–226. [CrossRef]
102. Verdan, S.; Theurillat, T.; Fachard, S.; Ghilardi, M. Of Dykes and Men: Eretria in the Making. In *Opere di Regimentazione delle Acque in Età Arcaica, Roma, Grecia e Magna Grecia, Etruria et Mondo Italico*; Bianchi, E., D'Acunto, M., Eds.; Edizioni Quasar: Rome, Italy, 2020; pp. 19–36.

103. Ghilardi, M.; Fachard, S.; Pavlopoulos, K.; Psomiadis, D.; Collana, C.; Bicket, A.; Crest, Y.; Bonneau, A.; Delanghe-Sabatier, D.; Knodel, A.; et al. Reconstructing Mid-to-Recent Holocene Paleoenvironments in the Vicinity of Ancient AMA-Rynthos (Euboea, Greece). *Geodin. Acta* **2012**, *25*, 38–51. [CrossRef]
104. Moody, J. Holocene Climate Change in Crete: An Archaeologist's View. In *Landscape and Land Use in Postglacial Greece. Sheffield Studies in Aegean Archaeology, 3*; Halstead, P., Frederick, C., Eds.; Sheffield Academic Press: Sheffield, UK, 2000; pp. 52–61.
105. Lemos, I.S. Euboea and Its Aegean Koine. In *Euboica: L'Eubea e la Presenza Euboica in Calcidica e in Occidente*; D'Agostino, B., Bats, M., Eds.; Centre Jean Bérard: Naples, Italy, 1998; pp. 45–58.
106. Kouli, K.; Triantaphyllou, M.; Pavlopoulos, K.; Tsourou, T.; Karkanas, P.; Dermitzakis, M.D. Palynological Investigation of Holocene Palaeoenvironmental Changes in the Coastal Plain of Marathon (Attica, Greece). *Geobios* **2009**, *42*, 43–51. [CrossRef]
107. Kvapil, L. The Agricultural Terraces of Korphos-Kalamianos: A Case Study of the Dynamic Relationship Between Land Use and Socio-Political Organization in Prehistoric Greece. Ph.D. Thesis, University of Cincinnati, Cincinnati, OH, USA, 2012.
108. Zangger, E. Landscape Changes around Tiryns During the Bronze Age. *Am. J. Archaeol.* **1994**, *98*, 189–212. [CrossRef]
109. Palaiologou, H. The Plain of Mycenae During the 13th Century BC and Later. In *Physis: Environnement Naturel et la Relation Homme-milieu dans le Monde Égéen Protohistorique, Proceeding of the Actes de la 14e Rencontre Égéenne International, Paris, France, 11–14 December 2012*; Touchais, G., Laffineur, R., Rougemont, F., Eds.; Leuven: Leuven, Belgium, 2014; Volume 34, pp. 517–519.
110. Maroukian, H.; Gaki-Papanastassiou, K.; Papanastassiou, D. Geomorphic and Seismotectonic Observations in the Area of Mycenae, Their Relation to the Catastrophes of Mycenae during Mycenaean Times. In *Archaeoseismology*; British School of Archaeology at Athens: Athens, Greece, 1996; pp. 189–194.
111. Zangger, E.; Timpson, M.E.; Yazvenko, S.B.; Kuhnke, F.; Knauss, J. The Pylos Regional Archaeological Project: Part II: Landscape Evolution and Site Preservation. *Hesperia J. Am. Sch. Class. Stud. Athens* **1997**, *66*, 549–641. [CrossRef]
112. Weiberg, E.; Bevan, A.; Kouli, K.; Katsianis, M.; Woodbridge, J.; Bonnier, A.; Engel, M.; Finné, M.; Fyfe, R.; Maniatis, Y.; et al. Long-Term Trends of Land Use and Demography in Greece: A Comparative Study. *Holocene* **2019**, *29*, 742–760. [CrossRef]
113. Emmanouilidis, A.; Panagiotopoulos, K.; Kouli, K.; Avramidis, P. Late-Holocene Paleoenvironmental and Land-Use Changes in Western Greece Based on a Sediment Record from Klisova Lagoon. *Holocene* **2022**, *32*, 485–500. [CrossRef]
114. Loizou, C. The Medieval Towers of Euboea: Their Dimension as Domestic and Landscape Phenomena. In *An Island between Two Worlds. The Archaeology of Euboea from Prehistoric to Byzantine Times*; Tankosic, Z., Mavridis, F., Kosma, M., Eds.; Norwegian Institute at Athens: Athens, Greece, 2017; Volume 6, pp. 625–638.
115. Dimiza, M.D.; Fatourou, M.; Arabas, A.; Panafiotopoulos, I.; Gogou, A.; Kouli, K.; Parinos, C.; Rousakis, G.; Triantaphyllou, M.V. Deep-Sea Benthic Foraminifera Record of the Last 1500 Years in the North Aegean Trough (Northeastern Mediterranean): A Paleoclimatic Reconstruction Scenario. *Deep.-Sea Res. Part II* **2020**, *171*, 104705. [CrossRef]
116. Bond, G.; Showers, W.; Cheseby, M.; Lotti, R.; Almasi, P.; deMenocal, P.; Priore, P.; Cullen, H.; Hajdas, I.; Bonani, G. A Pervasive Millennial-Scale Cycle in North Atlantic Holocene and Glacial Climates. *Science* **1997**, *278*, 1257–1266. [CrossRef]
117. Weiberg, E.; Unkel, I.; Kouli, K.; Holmgren, K.; Avramidis, P.; Bonnier, A.; Dibble, F.; Finné, M.; Izdebski, A.; Katrabtsiotis, C.; et al. The Socio-Environmental History of the Peloponnese during the Holocene: Towards an Integrated Understanding of the Past. *Quat. Sci. Rev.* **2016**, *136*, 40–65. [CrossRef]